Accepted in May 2018 at the *Journal of Human Evolution*

Trabecular bone patterning across the human hand

Nicholas B. Stephens [a,*], Tracy L. Kivell [b, a], Dieter H. Pahr [c], Jean-Jacques Hublin [a], Matthew M. Skinner [b, a]

[a] *Department of Human Evolution, Max Planck Institute for Evolutionary Anthropology, Deutscher Platz 6, 04103 Leipzig, Germany*

[b] *Skeletal Biology Research Centre, School of Anthropology and Conservation, University of Kent, Canterbury CT2 7NZ, United Kingdom*

[c] Institute for Lightweight Design and Structural Biomechanics, Vienna University of Technology, Getreidemarkt 9, A-1060 Vienna, Austria

[*] Corresponding author

E-mail address: nick_stephens@eva.mpg.de (N. B. Stephens)

Keywords: Hand evolution; Trabecular bone; Functional morphology; Biomechanics; Behavioral reconstruction; Histomorphometry

Abstract

Hand bone morphology is regularly used to link particular hominin species with behaviors relevant to cognitive/technological progress. Debates about the functional significance of differing hominin hand bone morphologies tend to rely on establishing phylogenetic relationships and/or inferring behavior from epigenetic variation arising from mechanical loading and adaptive bone modeling. Most research focuses on variation in cortical bone structure, but additional information about hand function may be provided through the analysis of internal trabecular structure. While primate hand bone trabecular structure is known to vary in ways that are consistent with expected joint loading differences during manipulation and locomotion, no study exists that has documented this variation across the numerous bones of the hand. We quantify the trabecular structure in 22 bones of the human hand (early/extant modern *Homo sapiens*) and compare structural variation between two groups associated with post-agricultural/industrial (post-Neolithic) and foraging/hunter-gatherer (forager) subsistence strategies. We (1) establish trabecular bone volume fraction (BV/TV), modulus (E), degree of anisotropy (DA), mean trabecular thickness (Tb.Th) and spacing (Tb.Sp); (2) visualize the average distribution of site-specific BV/TV for each bone; and (3) examine if the variation in trabecular structure is consistent with expected joint loading differences among the regions of the hand and between the groups. Results indicate similar distributions of trabecular bone in both groups, with those of the forager sample presenting higher BV/TV, E, and lower DA, suggesting greater and more variable loading during manipulation. We find indications of higher loading along the ulnar side of the forager sample hand, with high site-specific BV/TV distributions among the carpals that are suggestive of high

41 loading while the wrist moves through the ‘dart-thrower’s’ motion. These results support the
42 use of trabecular structure to infer behavior and have direct implications for refining our
43 understanding of human hand evolution and fossil hominin hand use.

Introduction

Interest in primate hand morphology and function is longstanding (e.g., Jones, 1916; Ashley-Montagu, 1931; Napier, 1960; Lewis, 1969; Susman, 1979; Diogo et al., 2012; Boyer et al., 2013), as the hand interacts with substrates during locomotion (e.g., Doran, 1993; Daver et al., 2012; Congdon and Ravosa, 2016) while also facilitating dexterous manipulation during social grooming (Whiten et al., 1999; Brand et al., 2017), food acquisition (Hunt, 1991; Boesch and Boesch, 1993; Visalberghi et al., 2009), communication (Hopkins et al., 2005; Zlatev, 2008), and complex object manipulations (Marzke and Wullstein, 1996; Viaro et al., 2017). Among primates, humans are often cited as the most dexterous (Napier, 1960; Vereecke and Wunderlich, 2016), possessing a suite of morphological features that allow for a wide range of wrist movements, power 'squeeze' grips (Marzke et al., 1992), and the formation of stable precision grips via the forceful opposition of the thumb and finger-pads (Napier, 1956; Marzke 1997; Susman, 1998). Early interpretations favored a view that human dexterity was derived, with researchers drawing strong causal links with hominin bipedal locomotion, the emergence of stone tool use, and/or increased carnivory (Young, 2003; Wood, 2014; Lemelin and Schmitt, 2016). Although most researchers still agree that the distinct aspects of human hand morphology are related to the selective pressures of at least three million years of tool-related behaviors (e.g., Napier, 1956; Washburn, 1960; Marzke, 1997; Harmand et al., 2015), there is less certainty about which features reflect a conserved ancestral state and which are derived (Tocheri et al., 2008; Rolian et al., 2010). This shift in our evolutionary understanding is the direct result of improved comparative techniques (Boyer et al., 2013; Almécija et al., 2015a; Boyer et al., 2015), new fossil discoveries (Kivell et al., 2011a, 2015; Lorenzo et al., 1999, 2015;

Almécija et al., 2012) and more comprehensive observational studies of non-human primate hand use (Hopkins et al., 2011; Marzke et al., 2015; Proffitt et al., 2016; Neufuss et al., 2017), which suggest that human-like hand morphology and use is more generalized and deep-rooted than previously appreciated (Alba et al., 2003; Almécija et al., 2010; Almécija and Alba, 2014; Rolian, 2016).

Thus, a greater understanding of how hand function may be reflected in hand morphology is needed. Variation in hand morphology has been key to informing hypotheses about not only manipulative behaviors and technological abilities in the human past (Leakey et al., 1964; Musgrave, 1971; Vlček, 1975; Susman, 1991, 1994; Niewoehner et al., 2003; Eren and Lycett, 2012; Wood, 2014), but also locomotor habits (Ricklan, 1987; Alba et al., 2003; Shrewsbury et al., 2003; Green and Gordon, 2008; Kivell, 2016), and—more indirectly—human neurological evolution and language acquisition (e.g., Falk, 1980; Hopkins, 2013; Putt et al., 2017). Interpreting hand function in the past is further complicated by the tendency for hominin fossil hand-remains to be recovered in isolation or as unassociated collections (Bush et al., 1982; Schmid and Berger, 1997; Venkataraman et al., 2013; Ward et al., 2014; Domínguez-Rodrigo et al., 2015; Lorenzo et al., 2015; Stratford et al., 2016; Daver et al., in press). As such, it is useful to explore methods with the potential to provide additional functional information about how manual behavior may have varied in the past that can also be applied to isolated hand bone elements.

Bone functional adaptation

Traditionally, researchers have compared the external shape of fossil hominin hand bones to generate hypotheses about hand function and grip capacity. For example, the potential for forming the precision and power grips observed during tool manufacture/use tend to be inferred from the hand proportions (i.e., thumb length relative to finger length) and shape of the trapezium-first metacarpal joint (e.g., Napier, 1962; Trinkaus, 1989; Godinot and Beard, 1991; Susman, 1994; Alba et al., 2003; Tocheri et al., 2003; Marzke et al., 2010). These morphological associations are established through observational studies focusing on wild and captive primate manipulative habits (e.g., Pouydebat et al., 2009, 2011, 2014; Bardo et al., 2015, 2016; Marzke et al., 2015; Orr, 2017), which provide the basis for understanding if extinct taxa with similar morphologies had similar manipulative capacities (e.g., Almécija et al., 2010; Almécija and Alba, 2014; Kivell et al., 2015; Orr, 2018). However, as external morphology only allows inferences about manipulative capacity, and not necessarily actual behavior, many researchers have begun to quantify epigenetic changes to bone that result from repetitive loading (e.g., compression, tension, and shear; Frost, 1987).

This phenomenon, commonly referred to as bone functional adaptation, has been experimentally observed to alter the structure in ways that improve the mechanical competence of repeatedly-loaded bone (Lanyon and Rubin, 1985; Pontzer et al., 2006; Ruff et al., 2006; Barak et al., 2011; Schulte et al., 2013; Christen et al., 2014; Cresswell et al., 2016; Christen and Muller, 2017; Ritter et al., 2017). For instance, cortical bone adjusts in thickness for improved resistance to bending forces, while trabecular bone alters the thickness, spacing, and orientation of struts adjacent to loaded regions in a way that enhances the transfer of kinetic energy away from joint surfaces (Cowin et al., 1985; Keaveny et al., 2001; Sugiyama et

al., 2010; Currey, 2011; Barak et al., 2013; Reznikov et al., 2015; but see Demes et al., 1998; Ozcivici and Judex, 2014; Wallace et al., 2015a, b; Fairfield et al., 2017). In general, many regions of the primate skeleton exhibit evidence of adaptive modeling, with structural variation aligning with hypothesized loading differences (e.g., Rafferty and Ruff, 1994; Ryan and Ketcham, 2002; Stock, 2006; Marchi and Shaw, 2011; Ryan and Shaw, 2012; Su et al., 2013; Chirchir, 2015; Fabre et al., 2017; Reznikov et al., 2017; Stieglitz et al., 2017), and hand bone variation reflecting known locomotor, postural, and manipulatory habits (e.g., Marchi, 2005; Patel and Carlson, 2007; Lazenby et al., 2008a, b,2011a; Zeininger et al., 2011; Tsegai et al., 2013; Barak et al., 2017; Chirchir et al., 2017b).

For hand trabecular bone, there are some studies that have reported ambiguous results between inferred loading and structure (e.g., Lazenby et al., 2011a; Schilling et al., 2014; Stephens et al., 2016a; Reina et al., 2017), with overlapping or unanticipated levels of bone volume fraction (BV/TV) and trabecular strut alignment (degree of anisotropy; DA). Explanations for such inconsistencies are found in well-controlled experiments, which utilize animal models to highlight how bone modeling may be influenced by genetic, systemic, or hormonal variation (e.g., Wallace et al., 2010, 2015a; Schlecht et al., 2014; Smith et al., 2014; Fairfield et al., 2017; see Wallace et al., 2017b for a recent review). Among humans, these factors are best understood as they relate to bone's role in maintaining homeostasis, with differences in bone structure arising from nutritional stress (e.g., anemia, pregnancy) or advanced age (e.g., menopause, osteoporosis; Agarwal, 2016). For trabecular bone these changes are documented in modern and archaeological contexts, with shifts from high BV/TV and low DA (more isotropic) to relatively low BV/TV and high DA (more anisotropic), which

prioritizes resistance to load along a singular axis (Singh et al., 1970; Agarwal et al., 2004; Christen et al., 2014; Beauchesne et al., 2017). Much of this understanding has come from the ability to perform more comprehensive quantitative analyses, which better characterize local micro-structural changes in bone (Poole et al., 2012; Gee and Treece, 2014; Gross et al., 2014; Hermann and Klein, 2015; Phillips et al., 2015). This is especially evident in trabecular studies, which have moved from single volume of interest (VOI) analyses to the simultaneous analyses of multiple VOIs (Su and Carlson, 2017; Sylvester et al., 2017) or the whole-bone/epiphysis (Gross et al., 2014; Taghizadeh et al., 2017).

For hand bones, such methods have documented differences in the distribution of trabeculae in the primate third metacarpal (Mc3) that align with predicted joint loading during locomotion and manipulation (Tsegai et al., 2013; Chirchir et al., 2017b; Barak et al., 2017). Other studies have identified similar distributions of BV/TV in human and fossil hominin metacarpals, which suggests a shared pattern of joint loading that may be related to opposition on the thumb during the use of precision grips (Skinner et al., 2015a, b; Stephens et al., 2016a; but see Almécija et al., 2015b). Such results establish the value of trabecular bone analysis to examine aspects of extant and fossil primate manual behavior, which we explore here through the quantification of trabeculae from the articulated elements of the wrist, metacarpus, and phalanges of human (*Homo sapiens*) hands (excluding the pisiform and distal phalanges).

To assess if trabecular architecture of the hand is related to differences in manipulatory loading, we follow previous analyses of other skeletal regions (e.g., Ryan and Shaw, 2015; Scherf et al., 2016; Stieglitz et al., 2017), and compare two groups of humans broadly defined by subsistence strategy and assumed behavior (i.e., community dwelling post-Neolithic

153 agriculturalists/industrialists and mixed foraging/hunter-gatherers; hereafter ‘post-Neolithic’
154 and ‘forager’, respectively). While these categories are reductionist given the
155 temporogeographically disparate sample (see methods), our aim here is to establish a
156 generalized view of trabecular distribution among the interrelated regions of the human hand.
157 If there are morphological differences attributable to variation in manipulative loading, then
158 these results should be useful in examining more refined questions about individual or group
159 differences in hand use (e.g., between males and females or across occupations; Macintosh et
160 al., 2014, 2017; Sládek 2016; Karakostis 2017), or joined with studies utilizing cortical mapping
161 and/or geometric morphometric techniques to address questions about skeletal variation in
162 complete, incomplete, or unassociated fossil hand remains (e.g., Ward et al., 2014; Domínguez-
163 Rodrigo et al., 2015; Lorenzo et al., 2015; Stratford et al., 2016). Predictions for how human
164 hand trabecular structure may vary follow after a brief review of human hand and wrist
165 kinematics.

166 Although the interactions at the base of the metacarpals are complex, a simplified
167 understanding may be reached by dividing the hand into radial, ulnar, and thumb portions,
168 according to their movement. The radial portion is rendered relatively immobile by a tight
169 binding of ligaments at the Mc2–Mc3 bases and CMC joint congruence (predominantly the
170 trapezoid and capitate; Brand and Hollister, 1993; Lazenby et al., 2008b; Tocheri et al., 2008).
171 The Mc4–Mc5 in the ulnar portion, however, share a complimentary articular surface with the
172 hamate, which allows these bones to rotate and translate as they flex up to 15 and 30º,
173 respectively (El-Shennawy et al., 2001; Lazenby et al., 2008a; Halilaj et al., 2014; Drapeau,
174 2015). Thumb opposition is a complex movement facilitated by the saddle-shaped TMC

articulation. Specifically, opposition of the thumb causes the Mc1 base to abduct, flex, rotate, and translate ulnarly across the trapezial surface (Halilaj et al., 2015), while the thenar musculature appears to prevent dislocation under load by locking it in place (Brand and Hollister, 1993; D'Agostino et al., 2017).

Potential loading differences

As with previous research, here we assume that variation in trabecular structure between the post-Neolithic and forager samples will be related to differences in activity levels (Polk, 2002; Rhodes and Knusel, 2005; Barak et al., 2011; Shaw et al., 2012; Rabey et al., 2015; Stieglitz et al., 2017; Wallace et al., 2017b). Similar inferences have been drawn in relation to skeletal variation within the lower and upper body, with highly mobile groups demonstrating a generally more robust skeletal structure as a result of repeated and higher loading than more recent humans (Trinkaus et al., 1994; Stock, 2006; Chirchir et al., 2015, 2017a; Ryan and Shaw 2015; Friedl et al., 2016; Scherf et al., 2016). The external morphology of *H. sapiens* hand bones has remained fairly stable from ~100 ka onward, with a notable reduction in morphological features associated with intense, repetitive loading being explained by humans shifting to more mechanically-advantaged technologies (e.g., TMC/Mc5 base; Niewoehner, 2001, 2006; Trinkaus, 2016). In this vein, Stock et al. (2013) reported low levels of right-side bias in the hunter-gatherer Mc2 cortical bone thickness (62.5%), relative to that of the humerus (83.6%), which contrasted with the fairly consistent right-side bias for both skeletal elements in the medieval and industrial samples. This result suggests more equally dispersed bimanual loading for the hunter-gatherer sample, which is consistent with hand use experiments documenting

high loading in the dominant or non-dominant hand during various subsistence activities (e.g., butchering, percussive activities; Rolian et al., 2011; Shaw et al., 2012; Key and Dunmore 2015; Key, 2016; Key et al., 2017; Williams-Hatala et al., 2017).

Following from this, variations in hand loading will most likely be related to grips and hand postures that invoke different levels of loading. For instance, less strenuous precision tasks tend to involve the pads of the fingers and only the dominant hand (e.g., low force, tip-to-tip pinch), while more strenuous tasks tend to involve stable grips (e.g., high force, key-grips and/or power grips) utilizing one or both hands (Marzke et al., 1998; Bullock et al., 2010; Williams et al., 2010; Key and Lycett, 2011, 2016; Borel et al., 2016). From these grips the muscle co-contraction and joint reaction forces are uniformly displaced into the radius and ulna during manipulation, with the radial side of the hand displacing most of the force (Gislason et al., 2009, 2010; Pataky et al., 2012; Chen et al., 2014; Márquez-Florez et al., 2015). Even so, high loading is present even during banal manipulations (e.g., pinch force during pipetting; Wu et al., 2015) and—given the physiological limits to modeling (Lambers et al., 2013; Cresswell et al., 2016; Yang et al., 2017)—this may result in generally similar trabecular parameters in the bones along the radial side of the hand (e.g., phalanges, Mc1, Mc2, trapezium, trapezoid). Instead, differences in loading may be more evident along the ulnar side of the hand, where kinetic energy is dissipated during strenuous manual activities that invoke the use of a power grip and involve wrist movements typified by the 'dart-thrower's' motion (e.g., throwing or hammering; Iwasaki et al., 1998; Young, 2003; Majima et al., 2008; Varga et al., 2013; Gabra and Li, 2016; Liu et al., 2016b; Rainbow et al., 2016). Aside from this, subtle differences in the distribution of

site-specific BV/TV may be discernable in various anatomical regions, with higher values indicating areas of localized modeling from frequent joint loading.

Predictions

Given the overall (presumed) similarity in hard and soft tissue morphology across all *H. sapiens*, we predict that the pattern of loading interpreted from the trabecular structure will be broadly similar between the two groups, i.e., (1) reflecting flexion at the interphalangeal joints; (2) flexion and adduction/abduction at the metacarpophalangeal joints; and (3) similar patterns of movement and loading at the TMC and intercarpal joints. However, previous research suggests that the trabecular structure of the hand in the forager sample should be consistent with greater levels of loading in the upper body and more variable hand use when compared to the post-Neolithic sample. Thus, we predict that (4) foragers will have on average higher BV/TV and elastic modulus (E) than the post-Neolithic sample, but lower DA due to more varied loading of the hand. Finally, we predict that (5) these differences in hand use will be reflected in how the trabeculae are distributed—e.g., higher site-specific BV/TV in functionally relevant locations, such as palmoulnar concentrations in the Mc2–Mc5 heads (Skinner et al., 2015a, b) and the palmoradial region of the Mc1 (Stephens et al., 2016a).

Materials and methods

Skeletal sample

Table 1 shows all manual skeletal elements of post-Neolithic and forager *H. sapiens* analyzed in this study. While sample sizes for some bones are small, this reflects the paucity of archaeological/paleontological remains with (relatively) complete hands available for microtomographic (µCT) scanning. The post-Neolithic sample is composed of 26 individuals, including associated hand skeletons of 10 Nubian Egyptians (6^{th}–11^{th} century; Strouhal and Jungwirth, 1979; Paoli et al., 1993), 10 individuals from a cemetery in Inden, Germany (18^{th}–19^{th} century), four from Medieval Canterbury, UK (11^{th}–15^{th} century; Hicks et al., 2001), and two from Syracuse, Sicily (20^{th} century). The forager sample is composed of 16 individuals, including associated and isolated remains of eight individuals from Tiera del Fuego (19^{th} century; Marangoni et al., 2011), eight individuals from Věstonice/Pavlov (~23 ka; Sládek, 2000), Arene Candide 2 (9900–10,850 uncal BP; Sparacello et al., 2015), one individual from Lapa do Santo, Brazil (~9.2 ka; Strauss et al., 2015), Barma Grande 2 (~24 Ka; Formicola et al., 1990; Churchill and Formicola, 1997), Ohalo II (~19 ka; Hershkovitz et al., 1995), and Qafzeh 8 and 9 (~80–130 ka; Schwarcz et al., 1988).

As pointed out by Friedl et al. (2016), the grouping of individuals from such a broad temporal range certainly obscures some subtle osteological differences, which should be kept in mind here. Still, a recent study of long-bone cross-sectional geometry likens the upper-limb activity patterns/levels of early *H. sapiens* (e.g., Qafzeh, Ohalo 2, and Gravettian) to contemporary forager samples (e.g., Khoesan), as opposed to Neanderthals (Pearson and Sparacello, 2017), which suggests that the manual loading among the forager sample would be similar enough for the main purposes of this analysis. Similarly, while some variation in manual loading and bone modeling may be related to sex and the sexual division of labor (e.g., Agarwal

2016; Macintosh 2014, 2017; but see Chirchir et al., 2017a), there are also issues with confidently attributing sex to early modern *H. sapiens* based on morphology alone (Mittnik et. al., 2016). Here the pooled sample is used to establish a general overview of trabecular variation that may then be subdivided into samples where there is higher confidence in the age, sex, occupation, and cultural affinity of the individuals.

MicroCT scanning

Microtomographic scans of the samples were obtained using either a SkyScan 1173 at 100–130 kV and 90–130 µA, a SkyScan 1176 scanner at 70 kV and 278 µA, a BIR ACTIS 225/300 scanner at 130 kV and 100–120 µA, or a Diondo d3 at 100–140 kV and 100–140 µA at an average isotopic voxel size of ~29 µm (range = 24–38 µm). Scans were reconstructed as 16-bit TIFF stacks, and each bone was isolated and reoriented to its approximate anatomical position in Avizo® 9.0 (FEI Visualization Sciences Group, Hillsboro, USA). During this process, the internal microstructure was visually assessed on a slice-by-slice basis and pathological or heavily damaged skeletal elements were removed from the sample. In the event that heavy sedimentation was present, manual removal was performed using a Wacom board (Coleman, 2003) and the Avizo paint-brush tool in the labels-field. In instances where the contrast between bone and sediment was impossible to distinguish, the entire section (e.g., the head or base of a metacarpal) was excluded from analyses (see Supplementary Online Material [SOM] Table S1).

Trabecular bone quantification and characterization

The methods employed in this study are described in detail elsewhere and are only briefly summarized here. An illustration of the workflow, along with the specific software packages, may be found in the SOM S1. In short, each bone was segmented using the Ray Casting Algorithm (Scherf and Tilgner, 2009) and then the script-based whole bone/epiphyseal approach Medtool v4.0 (Dr. Pahr Ingenieurs e.U, 2017; see below) was used to extract the cortical bone from the trabecular bone and generate a fine tetrahedral mesh representing the morphology of both tissues (Gross et al., 2014). Quantification of BV/TV, E, and DA of the trabecular mesh was performed in 3D by moving a 5 mm spherical VOI along a background grid with 2.5 mm spacing for each scan (Pahr and Zysset, 2009b), while mean trabecular thickness (Tb.Th, mm) and mean trabecular spacing (Tb.Sp, mm) were calculated following Hildebrand and Ruegsegger (1997). For further details see SOM S1 and SOM Figure. S1.

BV/TV is expressed as a percentage (bone voxels/total voxels), while DA is scaled between 1-0 (anisotropic-isotropic). We focus our analyses on these measures because previous studies show that they are not correlated with body mass (Doube et al., 2011; Barak et al., 2013; Ryan and Shaw, 2013) and are informative in regards to fracture resistance and relative arrangement (Maquer et al., 2015; Pahr and Zysset, 2009a, 2016). E is estimated using a reference tissue of E_0 = 10 GPa; ν_0 = 0.3; μ_0 = 3 GPa based on the Zysset-Curnier model (Zysset, 2003), which produces a more accurate measure by accounting for both BV/TV and fabric (Haïat et al., 2009; Latypova et al., 2017). This parameter identifies a material's mechanical ability to resist deformation under load (Zysset, 2003; Currey, 2011).

We compare these parameters for the whole carpal (capitate, hamate, lunate, scaphoid, trapezoid, trapezium, and triquetral), the heads (distal) and bases (proximal) of the metacarpals (Mc1–Mc5) and phalanges, including all proximal (PP1–PP5) and intermediate phalanges (IP2–IP5), and the distal phalanx (DP1) of the thumb. We exclude the pisiform and non-pollical distal phalanges due to the variable and miniscule trabeculae observed in the μCT scans, which was considered insufficient to allow for a robust calculation of the trabecular parameters (Pahr and Zysset, 2009a; Gross et al., 2012).

Due to shape variation among metacarpals and phalanges, each head/base segment was manually defined prior to analysis. To explore how trabecular structure may reflect differences in joint loading, each metacarpal head/base segment was subdivided into four regions at the radioulnar and dorsopalmar midlines (i.e., dorsoulnar, dorsoradial, palmoulnar, and palmoradial regions) and each phalangeal head/base segment was subdivided into two regions at the radioulnar midline (i.e., radial and ulnar regions). Trabecular parameters for each region were quantified using a Medtool script containing the dimensions of each bone segment.

Statistical analyses

Because of the interdependence of bones and muscles within the hand, we assume that many trabecular measurements may not be independent (e.g., BV/TV in the head of the metacarpal and the base of the articulating proximal phalanx). As such, we statistically tested our hypotheses using linear mixed effect models because they are able to compensate for underlying structures within the data (i.e., varying hierarchies; Lazic, 2010) through the

inclusion of random effects within the models (Barr et al., 2013). An example of this would be including the random effect of the 'individual' when there is data from bones of the right and left side. Table 2 defines the terms used to describe each model, while Figure 1 illustrates the three levels of comparison (head/base or carpal, metacarpal region, phalangeal region).

To explore variation among the regions of the hand and to help address the problem of non-independence more fully (i.e., reduce type I error), we defined functional groups for certain interrelated bones (e.g., thumb and rays II–V; see SOM S2 for further details). In addition, previous research has shown that there are significant differences between the head/base trabecular architecture of the Mc1, when compared to the Mc2–Mc5 (i.e., greater BV/TV and E with lower DA in the Mc1 head relative to the base while the reverse pattern has been found in the Mc2–Mc5; Lazenby et al., 2011a; Stephens et al., 2015, 2016b). For this reason, we ran models for the thumb bones (trapezium, Mc1, PP1, DP1) separately from the other bones in the hand (carpals, Mc2–Mc5, PP2–PP5, IP2–IP5). Violin plots were generated with the Seaborn v0.8.0 statistical data visualization package to compare distributions between variables (Waskom et al., 2017). All other statistical figures were generated with R v3.3.2 (R Core Team, 2016).

Model implementation

Six separate model setups were used to test for trabecular structure differences across regions of the hand. Each model was fitted using a Gaussian error structure and maximum likelihood (Bolker, 2008) using the lmer function within the lme4 package (Bates et al., 2014) for R. Each of the six model setups contained two models – a 'hand' subtype and 'thumb'

subtype – for each trabecular parameter compared (i.e., the response variables BV/TV, E, and DA).

Models in type 1 were run on data at the level of the bone and bone segment (i.e., metacarpal or phalangeal head and base, or carpal). Models in type 2 were run on data at the level of the metacarpal region (e.g., dorsoradial or palmoulnar regions of the Mc head and base) while models in type 3 used data at the level of the phalangeal region (i.e., radial and ulnar regions of the head and base). Each of these model types were further divided into two subtypes, based on data from the hand (i.e., not including the thumb; subtype a), and data from the thumb only (subtype b). Finally, two models were run for each subtype, one with BV/TV as the response variable and one with E as the response variable. Following Barr et al., (2013), all possible random slopes were included for these models. The specific steps followed for inclusion or rejection of each model are described in SOM S3. In all models, our primary aim was to test specifically for sample differences (post-Neolithic vs. forager) and, where applicable, differences by anatomical region. This included the potential for such differences to vary depending on the combination of sample, segment, and region being considered. In the same models, we also tested for whether there were any patterns across samples and segments or regions that differed based on the functional group being considered, but as these tests did not address our primary aim, the results are presented in SOM S4.

Type 1 model setup segment-level models. The type 1 models included data from bone segments (complete carpals, and metacarpal/phalangeal heads and bases). Subtype 1a included data derived from all bones of the hand, excluding those of the thumb. The two models in subtype 1a, each with a response variable of BV/TV or E, contained the predictors sample (post-

Neolithic vs. forager), segment (head, base, or carpal), side (left or right), and the sample-segment interaction. Additionally, we included random effects of functional group, skeletal element, specimen, hand ID (e.g., Qafzeh9-Left, or Arene Candide2-Right), and specific ID (i.e., identifying the specific bone; Table 2). The two models in subtype 1b included data from the bones of the thumb only, and all test predictors were the same as those in subtype 1a, aside from functional group as a random effect. The test predictors (i.e., the predictors of interest) for all four models in type 1 were sample and the sample-segment interaction. The secondary test predictors (i.e., those involving functional groups) were tested in subtype 1a models only and are described in the SOM S4 for model subtype 1a.

Type 2 model setup metacarpal region-level models. These models included data from the head/base regions of the metacarpals (dorsoulnar, dorsoradial, palmoulnar, palmoradial), with subtype 2a including data from Mc2–Mc5 and subtype 2b including data from Mc1 only. Both models in subtype 2a contained the predictors sample, segment, region (i.e., dorsoradial, dorsoulnar, palmoradial, or palmoulnar), side, and all two- and three-way interactions among sample, segment, and region. The random effects included were functional group, skeletal element, specimen, hand ID, specific ID, and region group (e.g., Qafzeh9-Left-Mc2-Base). The predictors for models in subtype 2b were identical to those in subtype 2a except for the exclusion of functional group and hand ID as random effects. Test predictors were all three- and two-way interactions, sample, and region for all models in type 2. All secondary test predictors from subtype 2a are described in SOM S4.

Type 3 model setup phalangeal region-level models. These included data at the level of the phalangeal head/base regions (ulnar and radial). Subtype 3a incorporated data from PP2–PP5

and IP2–IP5, while subtype 3b incorporated data from PP1 and the base of DP1. Subtype 3a models included as predictors sample, segment, region (i.e., radial or ulnar), side, and all two- and three-way interactions among sample, segment, and region. The random effects were functional group, skeletal element, specimen, hand ID, specific ID, and region group. Subtype 3b models were the same as those in subtype 3a, aside from functional group as a random effect. The test predictors for all type 3 models were identical to those for type 2. The secondary test predictors are described in SOM S4 for model subtype 3a.

Visual analysis

To compare sample differences in the distribution of site-specific BV/TV with morphologies that most closely approximate the actual shape variation between the post-Neolithic and forager bones, we used a custom Python 3.5 (Python Software Foundation) script to chain together slightly modified versions of the methods described in detail previously (Boyer et al., 2015; Gee et al., 2015; Tsegai and Stephens et al., 2017). A detailed illustration of the workflow, along with the specific software packages, is described in SOM S5 and SOM Figure S2**.** In short, we used modules within Medtool to interpolate and map site-specific BV/TV to the nearest elements of the mesh representing the trabecular volume (spacing 0.6 mm). Hereafter, each individual mesh was globally aligned and registered to a representative mesh for each bone (e.g., hamate). The deformation from the registration was then used to generate a statistical shape model (spacing 0.3 mm), which represents the 'mean-mesh' (Cootes and Graham, 1995; Joshi et al., 2016). We then registered the mean-mesh to each individual mesh,

411 and the corresponding site-specific BV/TV values at each vertex were then averaged for each
412 sample (e.g., all hamates in the forager sample) and mapped onto the mean-mesh.

413

414 **Results**

415 SOM Table S2 contains the carpal, metacarpal head/base, and phalangeal head/base
416 mean values and standard deviations for all of the trabecular parameters related to mechanical
417 properties (BV/TV, E, DA) and architecture (Tb.Th, Tb.Sp). The sample means for BV/TV, E, and
418 DA are illustrated by skeletal element in Figure 2, while those of Tb.Th and Tb.Sp are illustrated
419 in Figure 3. A heatmap depicting individual variation for BV/TV, E, and DA by bone and segment
420 is available in SOM Figure S3.

421 Models with BV/TV and E as the response variable successfully met all the model
422 assumptions, while those for DA were rejected because they did not meet the criteria for
423 normality and homogeneity of residuals (SOM Fig. S4). Therefore, we averaged the right/left DA
424 values for bones belonging to the same individual and performed a Mann-Whitney U pairwise
425 comparison between the post-Neolithic and forager samples for each bone or segment. The
426 significant results for the final models are summarized below, while the results for each of the
427 model comparisons are available in SOM Table S3.

428

429 *Sample differences in anisotropy*

430 SOM Table S4 contains the results of the Mann-Whitney U comparisons. Significant
431 differences were found for the lunate (post-Neolithic = 0.12, forager = 0.03; p = 0.043) and

triquetrum (post-Neolithic = 0.10, forager = 0.04; p = 0.028). A trend (i.e. marginal significance) was also identified for the Mc2 base (post-Neolithic = 0.17, forager = 0.12; p = 0.057) and Mc3 base (post-Neolithic = 0.17, forager = 0.10; p = 0.067). In each case this was the result of the post-Neolithic sample being more anisotropic than the foragers, which was the general pattern across the hand in all but the PP1 head, Mc5 head/base, and PP5 head/base. In general, DA was much more variable (i.e., high standard deviations; see SOM Table S2 and SOM Fig. S5) across the hand in both samples, compared with BV/TV and E (see below).

Sample differences in the segments for hand (1a) and thumb (1b) models

Model 1a investigated sample differences in BV/TV and E in bone segments of the hand (scaphoid, lunate, triquetral, hamate, capitate, trapezoid, and Mc2–Mc5, PP2–PP5, and IP2–IP5 head/base segments), while model 1b focused on the bone segments of the thumb (trapezium, Mc1 and IP1 head/base segments, and DP1 base segments). In all four models, we found a significant interaction between sample and segment (hand - BV/TV: p = 0.045; E: p = 0.030; thumb - BV/TV: p = 0.048; E: p = 0.026), indicating that the difference between the two samples varies depending on which segment is being considered (e.g., the difference in the Mc1 is different from that in the trapezium).

The model type 1 results are illustrated in SOM Figure S6. For both BV/TV and E, the forager sample has higher values than the post-Neolithic overall. However, while the differences are similar for the heads and bases, the differences in carpal BV/TV and E are more pronounced (Fig. 2; see also SOM Fig. S3). Figure 2 shows the respective distributions of BV/TV,

E, and DA for each carpal in each sample and—while both samples share a pattern of comparatively high BV/TV and E in the lunate, scaphoid, and capitate—the mean values for foragers are greater throughout the carpus. The greatest difference between the mean BV/TV and E for two samples is in the lunate, followed by the triquetral, capitate, and trapezium (see SOM table S2). The violin plots of each carpal illustrate the distributions for BV/TV, E, and DA for each of the two samples (Fig. 4). Given the similarity in mean trabecular spacing between the samples (Fig. 3), the identified interactions for BV/TV and E appear to be driven by generally thicker and more isotropic trabeculae in the carpus of the foragers, which is particularly pronounced in the lunate, capitate, triquetral, and trapezium.

Sample differences in the metacarpal regions for hand (2a) and thumb (2b) models

SOM Table S5 summarizes mean regional values of each sample by respective metacarpal or phalangeal head/base segment. For the models of the hand metacarpal regions (subtype 2a, head/base of Mc2–Mc5: dorsoradial, dorsoulnar, palmoradial, palmoulnar), we found a significant region-sample interaction for both response variables (BV/TV: $p = 0.002$, E: $p = 0.002$) as well as a significant region-segment interaction for BV/TV ($p = 0.013$). In the model of thumb metacarpal regions (subtype 2b, head/base Mc1: dorsoradial, dorsoulnar, palmoradial, palmoulnar), with BV/TV as the response variable we found a significant two-way interaction between sample and region ($p = 0.001$), as well as region and segment ($p < 0.001$), with a trend for the sample-segment interaction ($p = 0.074$). With E as the response variable, there was a trend for the three-way interaction between sample, region, and segment ($p = 0.076$).

Model type 2 results are illustrated in SOM Figures S7 and S8, while the mean BV/TV, E, and DA by head/base region are illustrated in Figure 5. For both samples, the head/base region pattern for BV/TV was very similar across the metacarpals (e.g., greater values in the Mc1 palmoradial region and Mc2–Mc4 palmoulnar region), and there was a tendency for the values in the Mc2 and Mc3 to be comparatively higher. Still, the forager sample showed consistently higher mean values, with the notable exception of the dorsoulnar and dorsoradial regions of the Mc1 base. Between the two samples, the differences were most marked in the palmoradial and palmoulnar regions of both head/base segments of the Mc1–Mc5 when compared to the dorsal regions, and this difference was exaggerated in the Mc2–Mc5 heads (SOM Fig. S7). The pattern for E across regions was, again, fairly similar between the samples for both the metacarpal heads and bases (Fig. 5) with the most striking differences appearing at the palmoulnar and palmoradial regions of the Mc1–Mc5 heads, where the forager sample showed much higher values (see also SOM Fig. S8). Again, there was a notable difference in the Mc1 dorsoulnar region of the base, with the post-Neolithic sample having greater values of E than the foragers.

Most differences between the two samples were related to the disparity between the various metacarpal regions. Architecturally (Fig. 3), there was little difference in mean Tb.Sp between the two samples while mean Tb.Th was notably thicker for the foragers at the base of the Mc3. The most marked differences between the two samples were in the distribution of mean DA among the metacarpal regions, which is relevant because E takes into account the fabric (i.e., the DA) as well as the BV/TV when it is calculated. Interestingly, for both samples the anisotropy pattern between the head/base segments of Mc5 was more similar to that of

the Mc1, with the head being more anisotropic than the base. The mean differences in DA by region (Fig. 5) show the foragers being more isotropic in the two palmar regions of the Mc1/Mc5, and two dorsal regions of the Mc3, but all Mc2 regions being anisotropic. At the base of the metacarpals, the forager sample was generally more isotropic in the Mc1–Mc4, but more anisotropic in the two ulnar regions of the Mc5. Taken together, the differences between the two samples were most pronounced in the Mc3 base, the palmar region of the Mc4 head/base, the palmoradial regions of the Mc5 base, and the palmoulnar/dorsoulnar regions of the Mc5 head.

Sample differences in the phalangeal regions for hand (3a) and thumb (3b) models

For hand models in subtype 3a (PP2–PP5 and IP2–IP5 head/base segments), we found that the forager sample had significantly higher BV/TV ($p = 0.018$) and E ($p = 0.016$) in the phalangeal bones of the hand. For thumb models in subtype 3b (PP1 head/base segments, and DP1 base segments), there was a trend for the difference between the samples in BV/TV ($p = 0.059$) and E ($p = 0.059$), with those of foragers being greater for both measures. Further, in thumb model 3b, we found a significant region-segment interaction for BV/TV ($p < 0.001$) and E ($p < 0.001$), where the values in the radial region were found to be higher than those in the ulnar region for both measures, with the variation in head being the most pronounced.

Model type 3 results are illustrated in the SOM Figure S9. Figure 5 shows the regional BV/TV, E, and DA means for each sample by skeletal element and segment, while violin plots comparing the regional differences in BV/TV and E are presented in the SOM Figures S10 and S11. Like the metacarpal regions above, the two samples were similar in that the higher BV/TV

519 and E values, along with lower DA values, were found in the central rays of the hand (rays II–IV).
520 There was also similarity in how BV/TV and E were distributed within the thumb, as suggested
521 by the interaction identified in the pollical phalanges. Here, the values on the radial side were
522 greater than the ulnar side in both samples, which appeared to be driven by the greater E and
523 BV/TV values in the head (SOM Figs. S10 and S11). As in the other bones, the regional means
524 for BV/TV and E were generally greatest in the forager sample, with those in the heads of the
525 various phalanges being the most different between the two samples, while those of the PP1,
526 DP1, and IP5 base were very similar. The greatest disparity between the samples was in rays II,
527 III, and V, particularly the heads of the intermediate phalanges. Architecturally, the two samples
528 share similar Tb.Sp throughout the hand (Fig. 3) and high DA at the base of PP5 and IP2 (Fig. 3).
529 Foragers had greater mean Tb.Th and lower DA in the heads of PP4 and MP4, as well as the PP1
530 base radial region.

531

532 *Visualized site-specific BV/TV*

533 Figure 7 presents a palmar and dorsal comparison for each sample of the average
534 surface site-specific BV/TV for each bone analyzed in this study, while an interactive mesh is
535 available in the online version or as a downloadable PLY file (SOM Model S1). There was a
536 general similarity between the two samples, but the forager sample differed in having higher
537 values (darker orange/red), which also tended to encompass a greater surface area than the
538 post-Neolithic sample (the extent of the orange/red borders). Differences between the two
539 samples were particularly marked in the carpals, along ray III, and in the heads of all the
540 phalanges. This is consistent with the statistical analyses reported above, with the forager

sample demonstrating significantly greater overall BV/TV and E, with values for DA being significantly different for the lunate and triquetral.

The color map of site-specific BV/TV across the phalanges is consistent with model results 3a and 3b (Fig. 7; also see above and Fig. 6). Both samples showed similarly high BV/TV values and distribution in the pollical phalanges and there was also a similar BV/TV distribution among the non-pollical phalanges, with greater values in the heads relative to the bases. Site-specific BV/TV values were greater in the forager sample overall, with the largest differences between the two samples found at the bases of the phalanges on the dorsal (PP2–PP4 and IP2–IP5) and palmar aspects (PP2–PP4), as well as the heads (PP3 and PP5 head ulnar region).

Figure 8 isolates the articular surfaces of the metacarpal heads and bases, showing patterns of site-specific BV/TV that are generally consistent with the results of metacarpal models 2a and 2b (see above), and the regional averages (Fig. 5). In both samples, the concentrations in the Mc1 were greatest in the radial regions of the head and base, while the heads of the non-pollical metacarpals showed a tendency towards higher values in the palmar-ulnar region. Although BV/TV mean values were, again, generally higher in the foragers, the pattern of BV/TV distribution was similar between the two samples. Compared with the post-Neolithic sample, foragers showed particularly high concentrations of BV/TV at the base of the Mc2 and Mc3, the palmar-radial portion of the Mc1 head, and the palmar-ulnar region of the Mc3 head.

For the hand and thumb models (1a and 1b), the significant differences were the result of variance in the carpals, with the forager sample demonstrating greater overall mean BV/TV and E. This difference was echoed in site-specific BV/TV color maps that highlight the sample

563 variation in the carpals from different anatomical views (Figs. 9 and 10). Along the distal carpal
564 row (trapezoid, capitate, hamate) there were similarities in the distribution of site-specific
565 BV/TV (i.e., ulnar aspect of the trapezoid, capitate head, and the triquetral and capitate facets
566 of the hamate), but the values for the foragers were much higher and more extensive,
567 particularly the radioulnar banding along the capitate head and the trapezoid-capitate
568 articulation (Fig. 10). These high BV/TV patterns correspond with those seen in distal view at
569 the midcarpal joint (Fig. 9), where high values were found in both samples along the dorsal
570 aspect of the lunate and ulnar aspect of the scaphoid articular surfaces, where they cup the
571 capitate head, but the patterns were more pronounced in the forager sample. In proximal view,
572 there were also BV/TV concentrations along the scaphoid and lunate at the radiocarpal joint in
573 both samples (Fig. 9), but with these patterns being much more pronounced in the proximal
574 and palmar surfaces of the lunate, as well as higher BV/TV in the triquetrum, compared with
575 the post-Neolithic sample. The forager sample also had a higher and more extensive BV/TV
576 distribution at the palmoulnar aspect of the trapezium's Mc1 facet, the capitate's Mc3 facet,
577 and the trapezoid's scaphoid facet (Figs. 7 and 9).

578

579 *Visualized across joint patterns*

580 Figure 11 shows a sagittal cross-sectional image of site-specific BV/TV through the
581 lunate, capitate, and bones of ray III (Mc3, PP3, IP3) for two post-Neolithic males from differing
582 locations but the same time period (19th century). Here the comparison is between individuals
583 with comparatively low (Fig. 11A) and high (Fig. 11B) BV/TV throughout the hand (see SOM Fig.
584 S12 for a comparison of trapezoids from multiple individuals). Along this articular chain there is

585 a good correspondence between the concentrations of relatively high site-specific BV/TV across
586 each joint. Overall the BV/TV distributions between the individuals are similar (e.g., high BV/TV
587 at the palmar metacarpophalangeal joint or dorsal lunate and central capitate head), but the
588 individual with high BV/TV differs in having high concentrations at the palmar capitate-Mc3
589 joint and in the palmar lunate.

590

591 **Discussion**

592 We examined the trabecular architecture within 22 of the 27 bones of the human hand
593 from a temporogeographically diverse collection of individuals with the aim of assessing if the
594 structural patterns across the joints were consistent with hand biomechanics. Additionally, we
595 categorized and compared individuals from a post-Neolithic and forager sample to see if the
596 variation between the two samples differed according to presumed differences in manipulative
597 loading. Given the comparable external morphology of recent *H. sapiens* (see Trinkaus, 2016),
598 we predicted that the general trabecular structure and site-specific BV/TV distributions would
599 be consistent with loading during flexion of the interphalangeal joints, flexion with abduction at
600 the metacarpophalangeal joints, and thumb opposition at the metacarpophalangeal and TMC
601 joints. In relation to sample differences, we predicted that the forager sample would have a
602 pattern consistent with higher and more variable manipulatory loading, which would be
603 reflected in higher average BV/TV, E, and lower average DA among the regions of the hand.
604 Furthermore, we predicted that these differences would be reflected in the distribution of site-
605 specific BV/TV, with higher values in the forager hand being consistent with areas of joint
606 contact observed during finger flexion, thumb opposition, and typical wrist movements.

607 Because previous studies have focused on hand bone trabecular architecture in isolated
608 elements (e.g., the Mc3 head) or limited regions of the hand (e.g., metacarpals; Lazenby et al.,
609 2011a; Zeininger et al., 2011; Schilling et al., 2014; Matarazzo, 2015; Skinner et al., 2015a; Barak
610 et al., 2017; Reina et al., 2017), we first summarize the general trabecular patterns across the
611 hand, and then present results on the non-pollical phalanges, metacarpals II–V, carpals, and
612 thumb. Following this, we discuss the interplay between hand loading, development,
613 demography, and individual variation across our samples.

614

615 *General pattern*

616 We found support for the predictions of similar hand use and wrist motion in the shared
617 distribution of trabeculae in the carpals, metacarpals, and phalanges of both the post-Neolithic
618 and forager samples. These similarities are suggestive of comparable joint contact and loading
619 as well as overall hand postures during manipulation, which is supported by studies of modern
620 humans showing that a limited number of hand grips are used for most daily tasks (Bullock et
621 al., 2010; Vergara et al., 2014; Liu et al., 2016b). More specifically, both samples demonstrated
622 a general pattern of high BV/TV and E in the heads of the Mc1 and the phalanges, when
623 compared to bases, and in the Mc2–Mc5 bases, when compared to the heads. Both samples
624 also shared a tendency to have relatively high BV/TV and E with lower DA throughout the
625 central portions of the hand (capitate, lunate, scaphoid, Mc2–Mc3, PP2–PP4, IP2–IP4). The site-
626 specific BV/TV for the post-Neolithic and forager samples, as well as the individual meshes (Fig.
627 11), also showed a good correspondence between concentrations of relatively high BV/TV and
628 areas of expected contact across joints (Figs. 7–11, SOM Fig. S12).

When the forager trabecular structure is compared to that of the post-Neolithic sample, the higher BV/TV, E, Tb.Th, site-specific BV/TV, and lower DA support our prediction that the forager sample would reflect a pattern of higher and more varied loading during hand use. BV/TV and E were significantly higher across the hand, the metacarpal/phalangeal segments, and the metacarpal/phalangeal regions, while DA was significantly lower for the lunate and triquetral (Figs. 2 and 3, SOM Figs. S6–S9). Variation in site-specific BV/TV was consistent with these significant differences, with the forager sample showing higher overall values, with the borders of the high BV/TV extending further across the joint surfaces. These differences were most pronounced in the carpals (scaphoid, lunate, capitate, triquetral, and trapezium), metacarpals (Mc1–Mc5 heads, Mc2–Mc3 bases), and phalanges (heads, and dorsal aspect of bases). These results are generally consistent with previous studies documenting more robust bone structure in upper and lower limb bones in active versus less active human samples (e.g., Stock, 2006; Ryan and Shaw, 2015; Scherf et al., 2016).

Finger phalanges

There is support for our prediction that the phalangeal trabecular structure would reflect flexion at the interphalangeal joints in both samples and that the forager sample would show evidence of greater loading overall. Both samples shared a pattern of relatively high BV/TV and E with low DA in the phalangeal heads when compared to the bases (Figs. 2 and 6, SOM Fig. S5), particularly in the central rays of the hand (II–IV). Higher BV/TV in the palmar regions of the proximal phalanges and dorsal regions of the intermediate phalanges in both samples is consistent with flexion of the interphalangeal joints. In each case, the forager sample

651 had lower DA overall, with significantly higher BV/TV and E throughout the phalanges. Taken
652 together, these results suggest general similarities in finger positioning during loading, but the
653 pattern for the forager sample hints at greater and more varied loading of the fingers, on
654 average. This may be related to variation in finger recruitment strategies, with the higher DA in
655 the post-Neolithic PP4–PP5 and IP2 bases signifying a consistency not present in the forager
656 sample (Fig. 2).

657 As far as we are aware, no other study has investigated human phalangeal trabecular
658 architecture (for African apes, see Matarazzo, 2015), but in both samples mean BV/TV and E
659 were generally greater in the distal segments of the phalanges (i.e., IP head > PP head; see SOM
660 Fig. S5). Overall this agrees with biomechanical studies measuring higher force and contact
661 pressures in the distal segments of the fingers during manipulation (Williams et al., 2012),
662 power grasping (Kargov et al., 2004; Goislard de Monsabert et al., 2012), and simulated
663 grasping (Chamoret et al., 2016). However, it conflicts with biomechanical modeling and
664 validation studies that report increasingly higher internal joint forces moving distal to proximal
665 along the phalanges (i.e., IP head < PP head < Mc head; Cooney and Chao, 1977; An et al., 1983,
666 1985). Thus, the head > base distribution of trabecular bone here is seemingly in conflict with
667 the distal < proximal joint force pattern. A partial explanation for this inconsistency may be
668 found in the force attentuation provided by soft tissues and variation in the articular surface
669 areas of the fingers (Rafferty and Ruff, 1994; Ruff, 2002; Diogo et al., 2012; Marzke, 2013;
670 Roberts and Konow, 2013; Hu et al., 2014). Studies quantifying the stiffness and compliance of
671 the fingers have shown how the joint capsules and musculotendon network of the hand act to
672 dissipate mechanical energy during impact to enhance grip stability while preventing injury

673 (Höppner et al., 2013, 2017; Fujihira et al., 2015; Deshpande et al., 2017). Qiu and Kamper
674 (2014) have also demonstrated that greater joint contact forces occur with more extreme
675 flexion (e.g., 60–90º), and that this force is greater in the distal joints due to the relative
676 reduction in tendon mass towards the fingertips (i.e., the proximal interphalangeal joint >
677 metacarpophalangeal joint). In other words, among the phalanges, manipulative activities that
678 require flexed fingers (i.e., power and precision grips) result in greater force than those with
679 straight fingers. Thus, the inconsistency between higher predicted load but lower trabecular
680 BV/TV and E throughout the phalanges is likely attributable to variation in joint angles during
681 manipulation and, in particular, the relatively large joint surface areas and more massive soft
682 tissue structures towards the proximal portions of the fingers that act to dissipate the higher
683 loads.

684

685 *Metacarpals II–V*

686 As with the phalanges, we found support for our prediction that both samples would
687 demonstrate similar loading patterns at the metacarpophalangeal and carpometacarpal joints,
688 but with more intense and varied loading in the forager sample. Both post-Neolithic and
689 forager samples generally showed greater mean BV/TV and E in the Mc2–Mc5 bases, when
690 compared to the heads (SOM Fig. S5). They also tended to have greater BV/TV, E, and Tb.Th but
691 lower DA in the central metacarpals (Mc2–Mc3; Figs. 2 and 5). The palmar regions of the Mc1–
692 Mc5 heads and bases had higher BV/TV and E, specifically the palmoulnar regions of Mc2–Mc5,
693 which is consistent with a flexed and adducted joint position of the proximal phalangeal bases
694 as the fingers and thumb rotate towards one another during opposition (Brand and Hollister,

1993). Again, the forager sample showed significantly higher BV/TV and E compared to the post-Neolithic sample, consistent with higher loading. These differences were most pronounced in the palmar regions of the Mc2–Mc4.

Our results are in keeping with previous studies that report an agreement between predicted loading history and metacarpal trabecular structure using VOI (Lazenby et al., 2008b; Chirchir et al., 2017b) and whole bone/epiphyseal methods (Tsegai et al., 2013; Skinner et al., 2015a). Our results contrast with Wong et al. (2017), who found that the dorsal, rather than palmar, region of the Mc2–Mc3 bases had generally higher trabecular bone mass and the Mc4–Mc5 showed a more homogeneous distribution across the base. However, this contradiction likely reflects the differing methodologies; whereas Wong et al. (2017) analyzed single tomographic slices using peripheral quantitative CT, we characterize the entire epiphyses. In the discussion, Wong et al., (2017) suggested that the more homogenous densities were likely related to the force attenuation provided by the tight articulation of the metacarpal bases and supportive ligaments. This interpretation is supported here with our finding of high concentrations of site-specific BV/TV between the Mc2/Mc3 and Mc4/Mc5 (Fig. 8), as well as concentrations along the dorsal surfaces of metacarpal bases that correspond to ligament attachment sites (Fig. 7).

Although the relationship between functional bone adaptation and musculotendon morphology is debatable (Vickerton et al., 2014; Rabey et al., 2015; Wallace et al., 2017a), the high site-specific BV/TV concentrations along the bases of the Mc2, Mc3, and Mc5, and those along the shaft of the Mc1 and Mc5, are consistent with muscle attachment sites related to flexion and opposition (Fig. 7; Brand and Hollister, 1993; Gislason et al., 2009; Diogo and Wood,

2011). For example, those at the palmar base of the Mc3 and along the dorsoradial shaft of the Mc1 and ulnar shaft of the Mc5 correspond to the attachment sites of the oblique head of the adductor pollicis, the opponens pollicis, and opponens digiti minimi respectively, which are thought to increase the mechanical effectiveness of the thumb and fifth finger during flexion (Marzke et al., 1998; Maki and Trinkaus, 2011). Similarly, high site-specific BV/TV along the palmar region of the Mc2 and the dorsal region of the Mc2–Mc3 correspond with the attachment sites of the flexor carpi radialis, extensor carpi radialis longus, and extensor carpi radialis brevis, which are important for controlling wrist flexion-extension and radioulnar deviation (Brand and Hollister, 1993). Considering that trabecular modeling events are found adjacent to the loaded site (Sugiyamat et al., 2010; Schulte et al., 2013; Christen et al., 2014; Cresswell et al., 2016) and that bone resists compressive forces better than tensile forces (Phillips et al., 2015), it may be that these site-specific BV/TV concentrations reflect modeling events initiated by tension transmitted to the bone when the muscles/ligaments work to counterbalance and stabilize the hand during manipulation. This interpretation is in line with other studies that note a relationship between attachment sites and changes in the bone microstructure of the hand (Karakostis and Lorenzo, 2016; Saffar, 2016), as well as Karakostis et al. (2017), who reported a significant relationship between human hand bone enthesis shape and occupations featuring high versus low manual loading.

Although both of our samples showed higher palmoulnar BV/TV, E, and site-specific BV/TV at the Mc2–Mc5 heads, the forager sample showed radial and dorsal expansion of these high values (Figs. 5, 7, and 8). For instance, the Mc5 of the forager sample showed relatively high site-specific BV/TV that extends along the dorsal aspect and ulnar lobe of the head. When

paired with the high DA along the dorsal region of the head and palmoulnar region of the base, this suggests a greater consistency in loading while the fifth digit is abducted, which would be consistent with wide grips involving broad/large objects (Goislard de Monsabert et al., 2014). The forager sample also had higher BV/TV, E, and site-specific BV/TV between the Mc2–Mc3 bases and, to a lesser extent, between the Mc4–Mc5 bases (Figs. 5 and 8). Along with the relatively low DA at the base of the Mc2–Mc4 and head of the Mc3, it may be that this pattern represents the distribution of high manipulative loading as the joints stabilize the hand (El-Shennawy et al., 2001; Buffi et al., 2013).

Carpals

For the carpals, both samples tended to have high values of BV/TV, E, and lower DA in the central elements (i.e., capitate, lunate, scaphoid; Fig.2) and similar distributions of site-specific BV/TV among the radiocarpal and midcarpal joints (Figs. 9 and 10), supporting our prediction of comparable patterns of joint contact. Our prediction regarding higher and more variable manual loading for the forager sample was supported by the significantly higher BV/TV, E, and lower DA in the carpals, as well as the visibly higher site-specific BV/TV concentrations observed along the scaphoid, lunate, capitate, and triquetral (Figs. 2, 9 and 10).

In relation to the predictions of wrist movement, the concentrations of site-specific BV/TV at the radiocarpal (proximal lunate and scaphoid) and midcarpal joints (distal lunate, distal scaphoid, and capitate head) are consistent with the load transfer and kinematics observations of carpals in motion (e.g., Crisco et al., 2005; Majima et al., 2008; Gislason et al., 2009, 2010; Rainbow et al., 2013; Márquez-Florez et al., 2015). More specifically, this pattern is

761 consistent with the kinematics of the carpals when moving between radial-extension and ulnar-
762 flexion as the wrist moves through the 'dart-thrower's' motion, which balances the tension
763 between the carpals in a manner that emphasizes motion at the midcarpal joint while
764 minimizing motion at the radiocarpal joint (Moojen et al., 2002a; Edirisinghe et al., 2014;
765 Rainbow et al., 2015). This movement characterizes the path that the wrist travels during many
766 high load tasks, such as short swing hammering, clubbing, and hard hammer knapping
767 (Leventhal et al., 2010; Garg et al., 2014; Williams et al., 2014), and is consistent with the
768 pattern of extremely low DA, high BV/TV, E, and Tb.Th in the forager capitate, lunate, and
769 scaphoid.

770 Following from this, the extremely low DA and high site-specific BV/TV in the forager
771 triquetral compared with the post-Neolithic sample may stem from loads incurred while
772 stabilizing the wrist during forceful manipulative activities. The high BV/TV on the palmoulnar
773 aspect of the triquetrum (Figs. 7 and 9) is consistent with attachment sites of the ligaments that
774 help to stabilize the ulnar wrist (Saffar, 2016). Similarly, the high BV/TV, E, and extremely low
775 DA for the trapezoid, capitate, and Mc2–Mc3 bases are consistent with derived articular
776 configuration of the *Homo* radial carpometacarpal complex, which helps distribute the high
777 joint reaction forces from the thumb (i.e., Mc3 styloid, and reoriented
778 Mc2/trapezoid/trapezium angles; Marzke, 1983, 1997; Tocheri et al., 2003, 2005, 2008; Ward et
779 al., 2014). More specifically, the presence of higher site-specific BV/TV values in the forager
780 trazpezoid-capitate articulation and those through the palmar aspect of the trapezoid (Fig. 10
781 and SOM Fig. S12) agree with the manner in which load is suggested to pass transerversly

782 through the expanded palmar aspect of the trapezoid during strong pinch/power grip (Tocheri
783 et al., 2005; Marzke et al., 2010).

784

785 *Thumb*

786 Both post-Neolithic and forager samples showed higher relative BV/TV and E in the
787 palmar and palmoradial regions of the Mc1, the radial regions of the pollical phalanges, and
788 high site-specific BV/TV at the trapeziometacarpal joint (Figs. 2, 6, and 9), which together are
789 consistent with the motion of the thumb during opposition to the other fingers (Nufer et al.,
790 2008; Lee et al., 2013; Ladd et al., 2014; D'Agostino et al., 2017). High site-specific BV/TV in the
791 palmar regions of the Mc1 is consistent with the area of joint contact at the TMC when the
792 thumb is opposed (Schneider et al., 2017), as well as the results of previous studies (Skinner et
793 al., 2015a; Stephens et al., 2016a; Wong et al., 2017). In contrast to other anatomical regions of
794 the hand, we did not find significant differences between the samples in levels of BV/TV and E
795 for the Mc1 or phalanges. While this suggests that thumb use was more similar for the two
796 samples than originally anticipated, the forager sample did show significantly higher BV/TV and
797 E in the trapezium (SOM Fig. S6). Furthermore, the high site-specific BV/TV expands further
798 across the trapezium's Mc1 articular surface and palmodorsally along the scaphoid articular
799 surface (Figs. 9 and 10). This pattern is consistent with the motion described by D'Agostino et
800 al., (2017), where the Mc1 base rotates during opposition of the thumb while the dorsoradial
801 ligament tightens in such a way that the palmar beak of the Mc1 base locks against the
802 palmoulnar region of the trapezium to stabilize the joint. When the higher regional BV/TV and E
803 in the palmar regions of the Mc1 base and the greater site-specific BV/TV on the palmoradial

804 aspect of the Mc1 base and head (Figs. 5, 7-9) are considered together, it may reflect loading
805 involving a widely abducted thumb (e.g., grasping a baseball as opposed to a pinch grip; Halilaj
806 et al., 2013, 2014). Given the specialized thenar musculature of the human thumb compared
807 with other primates (Diogo et al., 2012) —and the force-attenuating properties of soft tissue
808 discussed above—the higher E and BV/TV in the trapezium of the forager sample may reflect
809 higher loading of the thumb overall, with the joint contact forces ultimately being transferred
810 into the broad trapezial Mc1 facet, through to the scaphoid, and into the radius (Marzke et al.,
811 2010). This interpretation would be consistent with a similar transfer of kinetic energy during
812 power grips or strong pinch grips (Tocheri et al., 2003, 2005), as well the results discussed for
813 the remaining carpals above (e.g., the capitate-scaphoid border of the trapezoid).

814

815 *Developmental patterns*

816 Although our results are generally consistent with our predictions based on hand
817 kinematics, there are additional factors, such as ontogeny, that can influence trabecular
818 structure (Ryan et al., 2017). For instance, we found the metacarpal/phalangeal head and base
819 differences for BV/TV and E to be fairly uniform across individuals (see SOM Figs. S3 and S5),
820 which could be explained, at least in part, by development. Here the head/base distribution
821 mirrors the position of growth plates, which are located at the base of Mc1 and phalanges and
822 Mc2–Mc5 heads (Rolian, 2016; Perchalski et. al., 2017). Because new trabeculae are formed
823 only within the growth plate (Schulte et al., 2011), it seems somewhat contradictory that the
824 segments opposite the respective plates have the higher relative BV/TV, E, and Tb.Th (i.e.,
825 Mc1/phalangeal heads and Mc2–Mc5 bases; Figs. 2 and 3). For the phalanges this could

826 represent a biomechanical trade-off between epiphyseal cortical and trabecular bone (e.g.,
827 thicker PP1 base cortical bone allowing for lower BV/TV and E relative to the head). However,
828 Stephens et al. (2016b) found that these trabecular parameters covaried in human metacarpals,
829 such that higher BV/TV and E was paired with a thicker cortex in the Mc1 base and Mc2–Mc5
830 heads relative to their opposing segments.

831 In comparison to other primates, Matarazzo (2015) found that the trabecular structure
832 of the extant ape and macaque ray III (Mc3, PP3, and IP3) had a similar tendency for higher
833 BV/TV in the metacarpal/phalangeal heads when compared to the bases. However, there was
834 also substantial overlap in BV/TV values, with some individuals having higher BV/TV in the
835 bases, rather than the heads. While this difference may reflect systemic differences in
836 trabecular structure between humans and non-human primates (Tsegai et al., 2018) or
837 methodology (i.e., whole-bone/epiphysis approach vs. VOI), it may also reflect the high
838 locomotor loading of non-human primate hands compared with that of humans (Marchi, 2005;
839 Marzke et al., 2015). Since non-human primates have the same growth plate locations as
840 humans, this would suggest that loading can supersede a developmental predisposition. For the
841 human metacarpal/phalanges here, there are some BV/TV and E values that are nearly equal
842 between the head/base segments, with three phalanges where the base values are greater
843 than those of the head (SOM Fig. S5). This may mean that loads incurred during manipulation
844 are not high enough to cause frequent head/base variation, or that modeling is superimposed
845 onto the developmental architecture because typical loading of the hand follows this particular
846 pattern (e.g., higher joint force at the distal phalanges; Perchalski et al., 2017; Reina, 2007). In
847 either case, because modeling is limited to modulating trabecular thickness, spacing, and

orientation following epiphyseal fusion (Schulte et al., 2011; Barak et al., 2017), there is, at the very least, support for localized modeling among the differing Tb.Th, BV/TV, E, and site-specific BV/TV values (e.g., capitate, lunate, phalangeal heads, Mc3 base; Figs. 2 and 3). Still, these claims would be better substantiated if compared to a similar study involving an ontogenetic sample of human and non-human primates. Comparisons with foot bone trabecular structure, which have identical growth plate positions, could further test the influence of bone development on adult trabecular structure.

Demography and degree of anisotropy

Regarding comparisons of trabecular structure between the two samples, the results for DA are the most difficult to interpret because DA varies considerably compared to all other trabecular parameters (Tables 3 and 5, SOM Fig. S3). In other studies of human trabecular structure, the standard deviations of DA are generally low and comparable to those of BV/TV or Tb.Th, especially in the hands (e.g., Lazenby et al., 2008a, b, 2011a; Barak et al., 2017). Because DA characterizes the relative organization of trabeculae in 3D space—which will differ according to the anatomical region being analyzed—the high variability of DA we report likely relates to the methodological approach (Kivell et al., 2011b; Lazenby et al., 2011b). Namely, those that use single VOIs (Lazenby et al., 2008a, b, 2011a; Barak et al., 2017) versus other studies quantifying DA within the entire bone or epiphysis (Tsegai et al., 2013; Skinner et al., 2015a; Stephens et al., 2016), where the DA variation is similarly high. Considering the DA in the metacarpals here, where the larger bases vary more than the smaller heads (e.g., Mc2–Mc3), it may even be that larger volumes overgeneralize the measure. Being that controlled animal

studies demonstrate how struts align with loading axes (Pontzer et al., 2006; Barak et al., 2011), it may be more informative to visualize local differences in DA along with direction of alignment, which should reflect the primary direction of loading between joints (e.g., Tsegai et al., 2013; Barak et al., 2017).

That said, the bimodal distribution in the post-Neolithic carpals suggests a tendency towards either high or low DA (Fig. 4) that requires further investigation, ideally on osteological samples with known biological and occupational information. While we excluded all pathological bones and did not knowingly include individuals of advanced age, it may be that the high DA found in some individuals reflects age or physiological stress-related bias, which is characterized by low BV/TV and high DA (Agarwal, 2004, 2016; Beauchesne, 2017). When considering the large temporal differences between individuals in both samples, and the prevalence of nutritional stress/pathology regardless of subsistence strategy (e.g., Trinkaus et al., 2001; Macintosh et al., 2016), this is likely to have influenced the trabecular structure for some of the individuals in our sample. The inability of this analysis to both control for potentially confounding effects due to a lack of specific life history data (e.g., exact age, sex, occupation), as well as run linear mixed effect models on DA further complicates parsing out these fine-grained differences.

Further limitations

Although the aim of this study was to investigate for the first time the general patterns of trabecular structure across the human hand, there are several limitations to this study, in addition to ones discussed above, that should be underscored when considering the

892 interpretations above. Foremost are the limitations with our sample. As discussed above, we
893 divided up our sample into two broadly-defined groups that are temporogeographically diverse
894 and are not associated with direct life history information. Future analyses on a contemporary
895 sample or well-documented and temporally constrained archaeological sample would be useful
896 to see if the general patterns found here still hold (Karakostis et al., 2017; Reina et al., 2017;
897 Wong et al., 2017). Furthermore, one must consider bias stemming from preservation, such
898 that there are fewer individuals to be sampled in earlier time periods. This dearth of samples
899 complicates the number of reasonable divisions available during analysis, and we must keep in
900 mind that the earlier individuals may not truly be 'representative' of a particular population or
901 time period. For example, the forager individuals that overlap geographically, but not
902 necessarily temporally, show similar values, with Qafzeh 8 and 9 (130–80 ka) having
903 comparable values to the post-Neolithic means, while Arene Candide 2 (11–9 ka) and Barma
904 Grande 2 (24 ka) do not (SOM Fig. S3). While this is interesting and may be related to
905 similarities in terrain, culture, and/or genetic background, it is not a question that can be
906 adequately explored with the limited amount of Pleistocene remains available.

907 In relation to broader comparisons, we did not explore potential sex-related differences
908 in hand use. Bimanual humeral loading appears to have dramatically increased for females
909 compared to males following the adoption of agriculture (Macintosh et al., 2014, 2017; Sládek
910 et al., 2016), and it may be possible to assess if the right and left hands of females and males
911 from this period differed in consistent ways. Similarly, the functional interpretations here would
912 be better informed if accompanied by comparable data on non-human primate trabecular
913 bone. Although previous studies of isolated hand elements in non-human primates (e.g.,

914 Lazenby et al., 2011a; Schilling et al., 2013; Matazarro et al., 2015; Stephens et al., 2016a)
915 generally support the distinctive patterns of trabecular structure reported here for human
916 hands, such a comparison would allow for a more direct assessment of which aspects relate to
917 function and which relate to developmental, genetic, and/or age-related factors (e.g., Barak et
918 al., 2013; Ryan and Shaw, 2015; Agarwal, 2016).

919 Methodologically, it should be noted that calculation of E in this study is based on
920 computational simulations approximating μFE models experimentally validated using bones
921 other than those of the hand (e.g., femurs/vertebrae; Pahr and Zysset, 2009a,b; Schwiedrzik et
922 al., 2016). Further, while many of the trabecular patterns we found are consistent with what is
923 known about the biomechanics of the human hand, some functional interpretations are based
924 on simplified kinematic models due to the complexity of, for example, carpal movement (Crisco
925 et al., 2005; Gislason et al., 2009), and many of the complex interrelationships between hard
926 and soft tissues of the hand remain poorly understood (e.g., Landsmeer, 1955; Napier, 1960;
927 Crisco et al., 2005; Orr et al., 2010; Kivell et al., 2013; Saffar, 2016; Orr, 2017). Additionally, we
928 did not analyze variation in cortical bone, which has been shown to covary with trabecular
929 variables and is critical to how load is dissipated during manipulation (Tommasini et al., 2009;
930 Stephens et al., 2016b). While beyond the scope of this study, it would be fruitful to compare
931 individual site-specific BV/TV distributions to overlapping maps of DA, local orientation, Tb.Sp.,
932 Tb.Th., and cortical bone thickness (e.g., Tsegai et al., 2013; Barak et al., 2017; Tsegai and
933 Stephens et al., 2017), to gain a more holistic functional understanding of variation in bone
934 form.

935

Conclusions

This study aimed to describe for the first time the general patterns of trabecular structure across the human hand skeleton. The quantitative results and trabecular patterning described here were in line with our predictions of similar hand function between the post-Neolithic and forager samples. Higher BV/TV and E but generally lower DA in the forager sample suggests more intense and varied loading of the hands, on average. Using the site-specific BV/TV maps, we found good correspondence between the articulated elements of the hand, which helped to provide more in-depth interpretations of the quantitative data. Furthermore, the high site-specific BV/TV values were also consistent with the loading expected from in vivo observations of hand use. As such, analysis of trabecular structure and visualization of site-specific BV/TV across the human hand is both useful and relevant to debates about the reconstruction of manipulative behaviors in past samples and may be useful for interpreting fossil hominin remains. However, the functional interpretations made here should be tested on contemporary or archaeological samples of known behavior, and preferably within a broader comparative context of non-human primates.

Acknowledgements

This work was supported by the Max Planck Society (N.B.S., M.M.S., T.L.K., J.J.H.) and the European Research Council Starting Grant (grant number 336301; T.L.K. and M.M.S.). We are grateful for the samples provided by the Research Centre for Palaeolithics and Palaeoethnology, Věstonice (Jiří Svoboda), Museo Nazionale Preistorico dei Balzi Rossi (Elisabetta Starnini), the Museo Archeologico del Finale (Andrea De Pascale), the Sackler School

958 of Medicine at Tel Aviv University (Israel Herskovitz, Alon Barash, and Yoel Rak),
959 Naturhistorisches Museum Wien (Maria Teschler-Nicola and Ronald Muehl), the University of
960 Florence (Jacopo Moggi-Cecchi and Silvia Bortoluzzi), University of Kent (Chris Deter and Patrick
961 Mahoney), and the Johann-Friedrich-Blumenbach-Institut für Zoologie und Anthropologie der
962 Georg-August-Universität Göttingen (Birgit Großkopf). For scanning assistance, we thank David
963 Plotzki and Heiko Temming. For insightful discussions, we thank Colleen Stephens, Adam van
964 Casteren, and Zewdi Tsegai. We thank three anonymous reviewers and the editors of JHE for
965 comments that allowed for a much more nuanced interpretation of the results.

966 **References**

967 Agarwal, S.C., 2016. Bone morphologies and histories: Life course approaches in
968 bioarchaeology. American Journal of Physical Anthropology 159 S61, 130–149.

969 Agarwal, S.C., Dumitriu, M., Tomlinson, G.A., Grynpas, M.D., 2004. Medieval trabecular bone
970 architecture: the influence of age, sex, and lifestyle. American Journal of Physical
971 Anthropology 124, 33–44.

972 Alba, D.M., Moyà-Solà, S., Kohler, M., 2003. Morphological affinities of the *Australopithecus*
973 *afarensis* hand on the basis of manual proportions and relative thumb length. Journal of
974 Human Evolution 44, 225–254.

975 Almécija, S., Alba, D.M., 2014. On manual proportions and pad-to-pad precision grasping in
976 Australopithecus afarensis. Journal of Human Evolution 73, 88–92.

977 Almécija, S., Moyà-Solà, S., Alba, D.M., 2010. Early origin for human-like precision grasping: a
978 comparative study of pollical distal phalanges in fossil hominins. PLoS One 5, e11727.

979 Almécija, S., Alba, D.M., Moyà-Solà, S., 2012. The thumb of Miocene apes: new insights from
980 Castell de Barbera (Catalonia, Spain). American Journal of Physical Anthropology 148, 436–
981 450.

982 Almécija, S., Orr, C.M., Tocheri, M.W., Patel, B.A., Jungers, W.L., 2015a. Exploring phylogenetic
983 and functional signals in complex morphologies: the hamate of extant anthropoids as a test-
984 case study. The Anatomical Record 298, 212–229.

985 Almécija, S., Wallace, I.J., Judex, S., Alba, D.M., Moyà-Solà, S., 2015b. Comment on “Human-like
986 hand use in *Australopithecus africanus*”. Science 348, 1101.

An, K.N., Ueba, Y., Chao, E.Y., Cooney, W.P., Linscheid, R.L., 1983. Tendon excursion and moment arm of index finger muscles. Journal of Biomechanics 16, 419–425.

An, K.N., Chao, E.Y., Cooney, W.P., Linscheid, R.L., 1985. Forces in the normal and abnormal hand. Journal of Orthopaedic Research 3, 202–211.

Ashley-Montagu, F.M., 1931. On the primate thumb. American Journal of Physical Anthropology 15, 291–314.

Bain, G.I., Clitherow, H.D., Millar, S., Fraysse, F., Costi, J.J., Eng, K., McGuire, D.T., Thewlis, D., 2015. The effect of lunate morphology on the 3-dimensional kinematics of the carpus. Journal of Hand Surgery 40, 81–89.e1.

Barak, M.M., Lieberman, D.E., Hublin, J.J., 2011. A Wolff in sheep's clothing: trabecular bone adaptation in response to changes in joint loading orientation. Bone 49, 1141–1151.

Barak, M.M., Lieberman, D.E., Hublin, J.J., 2013. Of mice, rats and men: trabecular bone architecture in mammals scales to body mass with negative allometry. Journal of Structural Biology 183, 123–131.

Barak, M.M., Sherratt, E., Lieberman, D.E., 2017. Using principal trabecular orientation to differentiate joint loading orientation in the 3rd metacarpal heads of humans and chimpanzees. Journal of Human Evolution 113, 173–182.

Bardo, A., Borel, A., Meunier, H., Guery, J.P., Pouydebat, E., 2016. Behavioral and functional strategies during tool use tasks in bonobos. American Journal of Physical Anthropology 161, 125–140.

1007 Bardo, A., Pouydebat, E., Meunier, H., 2015. Do bimanual coordination, tool use, and body
1008 posture contribute equally to hand preferences in bonobos? Journal of Human Evolution 82,
1009 159–169.

1010 Barr, D.J., Levy, R., Scheepers, C., Tily, H.J., 2013. Random effects structure for confirmatory
1011 hypothesis testing: Keep it maximal. Journal of Memory and Language 68, 255–278.

1012 Bates, D., Mächler, M., Bolker, B., Walker, S., 2015. Fitting linear mixed-effects models using
1013 lme4. Journal of Statistical Software 67, 1—48.

1014 Beauchesne, P., Agarwal, S.C., 2017. A multi-method assessment of bone maintenance and loss
1015 in an Imperial Roman population: Implications for future studies of age-related bone loss in
1016 the past. American Journal of Physical Anthropology 164, 41–61.

1017 Boesch, C., Boesch, H., 1993. Different hand postures for pounding nuts with natural hammers
1018 by wild chimpanzees. In: Preuschoft, H., Chivers, D.J. (Eds.), Hands of Primates. Springer
1019 Vienna, Vienna, pp. 31–43.

1020 Bolker, B.M., 2008. Ecological Models and Data in R. Princeton University Press, Princeton.

1021 Borel, A., Chèze, L., Pouydebat, E., 2016. Sequence analysis of grip and manipulation during tool
1022 using tasks: a new method to analyze hand use strategies and examine human specificities.
1023 Journal of Archaeological Method and Theory 24, 751–775.

1024 Boyer, D.M., Puente, J., Gladman, J.T., Glynn, C., Mukherjee, S., Yapuncich, G.S., Daubechies, I.,
1025 2015. A new fully automated approach for aligning and comparing shapes. The Anatomical
1026 Record 298, 249–276.

1027 Boyer, D.M., Yapuncich, G.S., Chester, S.G., Bloch, J.I., Godinot, M., 2013. Hands of early
1028 primates. American Journal of Physical Anthropology 152 S57, 33–78.

1029 Brand, C.M., Marchant, L.F., Boose, K.J., White, F.J., Rood, T.M., Meinelt, A., 2017. Laterality of
1030 grooming and tool use in a group of captive bonobos (*Pan paniscus*). Folia Primatologica 88,
1031 210–222.

1032 Brand, P.W., Hollister, A., 1993. Clinical Mechanics of the Hand. Mosby Year Book, St. Louis.

1033 Buffi, J.H., Crisco, J.J., Murray, W.M., 2013. A method for defining carpometacarpal joint
1034 kinematics from three-dimensional rotations of the metacarpal bones captured in vivo using
1035 computed tomography. Journal of Biomechanics 46, 2104–2108.

1036 Bullock, I.M., Zheng, J.Z., De La Rosa, S., Guertler, C., Dollar, A.M., 2013. Grasp frequency and
1037 usage in daily household and machine shop tasks. IEEE Transaction on Haptics 6, 296-308.

1038 Bush, M.E., Lovejoy, C.O., Johanson, D.C., Coppens, Y., 1982. Hominid carpal, metacarpal, and
1039 phalangeal bones recovered from the Hadar formation: 1974-1977 collections. American
1040 Journal of Physical Anthropology 57, 651–677.

1041 Cardozo, D.F., Plata, G.V., Casas, J.A., Rodriguez, N.S., 2016. Acute dislocation of the
1042 metacarpal-trapezoid joint. Clinics in Orthopedic Surgery 8, 223–227.

1043 Chamoret, D., Bodo, M., Roth, S., 2016. A first step in finite-element simulation of a grasping
1044 task. Computer Assisted Surgery 21, 22–29.

1045 Chen, Y.R., Wu, Y.F., Tang, J.B., Giddins, G., 2014. Contact areas of the scaphoid and lunate with
1046 the distal radius in neutral and extension: correlation of falling strategies and distal radial
1047 anatomy. Journal of Hand Surgery Europe 39, 379–383.

1048 Chirchir, H., 2015. A comparative study of trabecular bone mass distribution in cursorial and
1049 non-cursorial limb joints. The Anatomical Record 298, 797–809.

1050 Chirchir, H., Ruff, C.B., Junno, J.A., Potts, R., 2017a. Low trabecular bone density in recent
1051 sedentary modern humans. American Journal of Physical Anthropology 162, 550–560.

1052 Chirchir, H., Zeininger, A., Nakatsukasa, M., Ketcham, R.A., Richmond, B.G., 2017b. Does
1053 trabecular bone structure within the metacarpal heads of primates vary with hand posture?
1054 Comptes Rendus Palevol 16, 533–544.

1055 Christen, P., Ito, K., Ellouz, R., Boutroy, S., Sornay-Rendu, E., Chapurlat, R.D., van Rietbergen, B.,
1056 2014. Bone remodelling in humans is load-driven but not lazy. Nature Communications 5,
1057 4855.

1058 Christen, P., Muller, R., 2017. In vivo visualisation and quantification of bone resorption and
1059 bone formation from time-lapse imaging. Current Osteoporosis Reports 15, 311–317.

1060 Churchill, S.E., Formicola, V., 1997. A case of marked bilateral asymmetry in the upper limbs of
1061 an upper palaeolithic male from Barma Grande (Liguria), Italy. International Journal of
1062 Osteoarchaeology 7, 18–38.

1063 Coleman, C., 2003. “Digital inking”: how to make perfect line drawings on computers.
1064 Organisms Diversity and Evolution 3, 303–304.

1065 Congdon, K.A., Ravosa, M.J., 2016. Get a grip: substrate orientation and digital grasping
1066 pressures in strepsirrhines. Folia Primatologica 87, 224–243.

1067 Cooney, W.P., 3rd, Chao, E.Y., 1977. Biomechanical analysis of static forces in the thumb during
1068 hand function. Journal of Bone and Joint Surgery 59, 27–36.

1069 Cootes, T.F., Taylor, C.J., Cooper, D.H., Graham, J., 1995. Active Shape Models-Their Training
1070 and Application. Computer Vision Image and Understanding 61, 38-59.

1071 Cowin, S.C., 1985. The relationship between the elasticity tensor and the fabric tensor.
1072 Mechanics of Materials 4, 137–147.

1073 Cowin, S.C., Hart, R.T., Balser, J.R., Kohn, D.H., 1985. Functional adaptation in long bones:
1074 establishing in vivo values for surface modeling rate coefficients. Journal of Biomechanics 18,
1075 665–684.

1076 Cresswell, E.N., Goff, M.G., Nguyen, T.M., Lee, W.X., Hernandez, C.J., 2016. Spatial relationships
1077 between bone formation and mechanical stress within cancellous bone. Journal of
1078 Biomechanics 49, 222–228.

1079 Crisco, J.J., Coburn, J.C., Moore, D.C., Akelman, E., Weiss, A.P., Wolfe, S.W., 2005. In vivo
1080 radiocarpal kinematics and the dart thrower's motion. Journal of Bone and Joint Surgery 87,
1081 2729–2740.

1082 Currey, J.D., 2011. The structure and mechanics of bone. Journal of Materials Science 47, 41–
1083 54.

1084 Cutkosky, M.R., Howe, R.D., 1990. Human grasp choice and robotic grasp analysis. In:
1085 Venkataraman, S.T., Iberall, T. (Eds.), Dextrous Robot Hands. Springer-Verlag, New York, pp.
1086 5–31.

1087 D'Agostino, P., Dourthe, B., Kerkhof, F., Stockmans, F., Vereecke, E.E., 2017. In vivo kinematics
1088 of the thumb during flexion and adduction motion: Evidence for a screw-home mechanism.
1089 Journal of Orthopaedic Research 35, 1556–1564.

1090 Daver, G., Berillon, G., Grimaud-Herve, D., 2012. Carpal kinematics in quadrupedal monkeys:
1091 towards a better understanding of wrist morphology and function. Journal of Anatomy 220,
1092 42–56.

1093 Daver, G., Berillon, G., Jacquier, C., Ardagna, Y., Yadeta, M., Maurin, T., Souron, A., Blondel, C.,
1094 Coppens, Y., Boisserie, J. R., in press. New hominin postcranial remains from locality OMO
1095 323, Shungura Formation, Lower Omo Valley, southwestern Ethiopia. Journal of Human
1096 Evolution. https://doi.org/10.1016/j.jhevol.2018.03.011.

1097 Demes, B., Stern, J.T., Jr., Hausman, M.R., Larson, S.G., McLeod, K.J., Rubin, C.T., 1998. Patterns
1098 of strain in the macaque ulna during functional activity. American Journal of Physical
1099 Anthropology 106, 87–100.

1100 Deshpande, A., Niehues, T., Rao, P., 2017. Implementation of human-like joint stiffness in
1101 robotics hands for improved manipulation. In: Ueda, J., Kurita, Y. (Eds.), Human Modelling
1102 for Bio-Inspired Robotics. Academic Press, London, pp. 3–35.

1103 Diogo, R., Richmond, B.G., Wood, B., 2012. Evolution and homologies of primate and modern
1104 human hand and forearm muscles, with notes on thumb movements and tool use. Journal of
1105 Human Evolution 63, 64–78.

1106 Diogo, R., Wood, B., 2011. Soft-tissue anatomy of the primates: phylogenetic analyses based on
1107 the muscles of the head, neck, pectoral region and upper limb, with notes on the evolution
1108 of these muscles. Journal of Anatomy 219, 273–359.

1109 Domínguez-Rodrigo, M., Pickering, T.R., Almécija, S., Heaton, J.L., Baquedano, E., Mabulla, A.,
1110 Uribelarrea, D., 2015. Earliest modern human-like hand bone from a new >1.84-million-year-
1111 old site at Olduvai in Tanzania. Nature Communications 6, 7987.

1112 Doran, D.M., 1993. Comparative locomotor behavior of chimpanzees and bonobos: the
1113 influence of morphology on locomotion. American Journal of Physical Anthropology 91, 83–
1114 98.

1115 Doube, M., Klosowski, M.M., Wiktorowicz-Conroy, A.M., Hutchinson, J.R., Shefelbine, S.J., 2011.
1116 Trabecular bone scales allometrically in mammals and birds. Proceedings of the Royal
1117 Society B 278, 3067–3073.

1118 Dr. Pahr Ingenieurs e.U., 2017. Medtool v4.0. Dr. Pahr Ingenieurs e.U., Pfaffstätten.
1119 http://www.dr-pahr.at.

1120 Drapeau, M.S., 2015. Metacarpal torsion in apes, humans, and early *Australopithecus*:
1121 implications for manipulatory abilities. PeerJ. 3, e1311.

1122 Edirisinghe, Y., Troupis, J.M., Patel, M., Smith, J., Crossett, M., 2014. Dynamic motion analysis of
1123 dart throwers motion visualized through computerized tomography and calculation of the
1124 axis of rotation. Journal of Hand Surgery Europe 39, 364–372.

1125 El-Shennawy, M., Nakamura, K., Patterson, R.M., Viegas, S.F., 2001. Three-dimensional
1126 kinematic analysis of the second through fifth carpometacarpal joints. Journal of Hand
1127 Surgery 26, 1030–1035.

1128 Eren, M.I., Lycett, S.J., 2012. Why Levallois? A morphometric comparison of experimental
1129 "preferential" Levallois flakes versus debitage flakes. PLoS One 7, e29273.

1130 Fabre, A.C., Marigó, J., Granatosky, M.C., Schmitt, D., 2017. Functional associations between
1131 support use and forelimb shape in strepsirrhines and their relevance to inferring locomotor
1132 behavior in early primates. Journal of Human Evolution 108, 11–30.

1133 Fairfield, H., Rosen, C.J., Reagan, M.R., 2017. Connecting bone and fat: the potential role for
1134 sclerostin. Current Molecular Biology Reports 3, 114–121.

1135 Falk, D., 1980. Language, handedness, and primate brains: did the australopithecines sign?
1136 American Anthropologist 82, 72–78.

1137 FEI Science Visualization Group, 2017. Avizo 9.0. FEI Science Visualization Group, Hillsboro.
1138 http://www.fei.com.

1139 Formicola, V., Frayer, D.W., Heller, J.A., 1990. Bilateral absence of the lesser trochanter in a late
1140 Epigravettian skeleton from Arene Candide (Italy). American Journal of Physical
1141 Anthropology 83, 425–437.

1142 Freivalds, A., 2011. Biomechanics of the Upper Limbs: Mechanics, Modeling and
1143 Musculoskeletal Injuries, 2nd ed. CRC press, New York.

1144 Friedl, L., Eisova, S., Holliday, T.W., 2016. Re-evaluation of Pleistocene and Holocene long bone
1145 robusticity trends with regards to age-at-death estimates and size standardization
1146 procedures. Journal of Human Evolution 97, 109–122.

1147 Frost, H.M., 1987. Bone “mass” and the “mechanostat”: a proposal. The Anatomical Record
1148 219, 1–9.

1149 Fujihira, Y., Harada, K., Tsuji, T., Watanabe, T., 2015. Experimental investigation of effect of
1150 fingertip stiffness on resistible force in grasping. In: 2015 IEEE International Conference on
1151 Robotics and Automation (ICRA). IEEE, Seattle, pp. 4334–4340.

1152 Gabra, J.N., Li, Z.M., 2016. Three-dimensional stiffness of the carpal arch. Journal of
1153 Biomechanics 49, 53–59.

1154 Garg, R., Kraszewski, A.P., Stoecklein, H.H., Syrkin, G., Hillstrom, H.J., Backus, S., Lenhoff, M.L.,
1155 Wolff, A.L., Crisco, J.J., Wolfe, S.W., 2014. Wrist kinematic coupling and performance during
1156 functional tasks: effects of constrained motion. Journal of Hand Surgery 39, 634–642.e1.

1157 Gee, A.H., Treece, G.M., 2014. Systematic misregistration and the statistical analysis of surface
1158 data. Medical Image Analysis 18, 385–393.

1159 Gee, A.H., Treece, G.M., Tonkin, C.J., Black, D.M., Poole, K.E., 2015. Association between femur
1160 size and a focal defect of the superior femoral neck. Bone 81, 60–66.

1161 Gislason, M.K., Nash, D.H., Nicol, A., Kanellopoulos, A., Bransby-Zachary, M., Hems, T., Condon,
1162 B., Stansfield, B., 2009. A three-dimensional finite element model of maximal grip loading in
1163 the human wrist. In: Proceedings of the Institution of Mechanical Engineers. Part H. Journal
1164 of Engineering in Medicine 223, 849–861.

1165 Gislason, M.K., Stansfield, B., Nash, D.H., 2010. Finite element model creation and stability
1166 considerations of complex biological articulation: The human wrist joint. Medical
1167 Engineering and Physics 32, 523–531.

1168 Godinot, M., Beard, K.C., 1991. Fossil primate hands: A review and an evolutionary inquiry
1169 emphasizing early forms. Human Evolution 6, 307–354.

1170 Goislard de Monsabert, B., Rossi, J., Berton, E., Vigouroux, L., 2012. Quantification of hand and
1171 forearm muscle forces during a maximal power grip task. Medicine and Science in Sports and
1172 Exercise 44, 1906–1916.

1173 Goislard de Monsabert, B., Vigouroux, L., Bendahan, D., Berton, E., 2014. Quantification of
1174 finger joint loadings using musculoskeletal modelling clarifies mechanical risk factors of hand
1175 osteoarthritis. Medical Engineering and Physics 36, 177–184.

1176 Green, D.J., Gordon, A.D., 2008. Metacarpal proportions in *Australopithecus africanus*. Journal
1177 of Human Evolution 54, 705–719.

1178 Gross, T., Kivell, T.L., Skinner, M.M., Nguyen, N.H., Pahr, D.H., 2014. A CT-image-based
1179 framework for the holistic analysis of cortical and trabecular bone morphology.
1180 Palaeontologia Electronica 17, 33A.

1181 Gross, T., Pahr, D.H., Peyrin, F., Zysset, P.K., 2012. Mineral heterogeneity has a minor influence
1182 on the apparent elastic properties of human cancellous bone: a SRmuCT-based finite
1183 element study. Computer Methods in Biomechanics and Biomedical Engineering 15, 1137–
1184 1144.

1185 Haïat, G., Padilla, F., Svrcekova, M., Chevalier, Y., Pahr, D., Peyrin, F., Laugier, P., Zysset, P.,
1186 2009. Relationship between ultrasonic parameters and apparent trabecular bone elastic
1187 modulus: a numerical approach. Journal of Biomechanics 42, 2033–2039.

1188 Halilaj, E., Moore, D.C., Patel, T.K., Ladd, A.L., Weiss, A.P., Crisco, J.J., 2015. Early osteoarthritis
1189 of the trapeziometacarpal joint is not associated with joint instability during typical isometric
1190 loading. Journal of Orthopaedic Research 33, 1639–1645.

1191 Halilaj, E., Rainbow, M.J., Got, C., Schwartz, J.B., Moore, D.C., Weiss, A.P., Ladd, A.L., Crisco, J.J.,
1192 2014. In vivo kinematics of the thumb carpometacarpal joint during three isometric
1193 functional tasks. Clinical Orthopaedics and Relatated Research 472, 1114–1122.

1194 Halilaj, E., Rainbow, M.J., Got, C.J., Moore, D.C., Crisco, J.J., 2013. A thumb carpometacarpal
1195 joint coordinate system based on articular surface geometry. Journal of Biomechanics 46,
1196 1031–1034.

1197 Harmand, S., Lewis, J.E., Feibel, C.S., Lepre, C.J., Prat, S., Lenoble, A., Boes, X., Quinn, R.L.,
1198 Brenet, M., Arroyo, A., Taylor, N., Clement, S., Daver, G., Brugal, J.P., Leakey, L., Mortlock,
1199 R.A., Wright, J.D., Lokorodi, S., Kirwa, C., Kent, D.V., Roche, H., 2015. 3.3-million-year-old
1200 stone tools from Lomekwi 3, West Turkana, Kenya. Nature 521, 310–315.

1201 Hermann, M., Klein, R., 2015. A visual analytics perspective on shape analysis: State of the art
1202 and future prospects. Computers and Graphics 53, 63–71.

1203 Hershkovitz, I., Speirs, M.S., Frayer, D., Nadel, D., Wish-Baratz, S., Arensburg, B., 1995. Ohalo II
1204 H2: a 19,000-year-old skeleton from a water-logged site at the Sea of Galilee, Israel.
1205 American Journal of Physical Anthropology 96, 215–234.

1206 Hicks, M., Hicks, A., 2001. St Gregory's priory, Northgate, Canterbury: Excavations 1988-1991.
1207 Canterbury Archaeological Trust Limited, Canterbury.

1208 Hildebrand, T., Ruegsegger, P., 1997. A new method for the model-independent assessment of
1209 thickness in three-dimensional images. Journal of Microscopy 185, 67–75.

1210 Hopkins, W.D., 2013. Neuroanatomical asymmetries and handedness in chimpanzees (Pan
1211 troglodytes): a case for continuity in the evolution of hemispheric specialization. Annals of
1212 the New York Academy of Sciences 1288, 17–35.

1213 Hopkins, W.D., Phillips, K.A., Bania, A., Calcutt, S.E., Gardner, M., Russell, J., Schaeffer, J.,
1214 Lonsdorf, E.V., Ross, S.R., Schapiro, S.J., 2011. Hand preferences for coordinated bimanual
1215 actions in 777 great apes: implications for the evolution of handedness in hominins. Journal
1216 of Human Evolution 60, 605–611.

1217 Hopkins, W.D., Russell, J., Freeman, H., Buehler, N., Reynolds, E., Schapiro, S.J., 2005. The
1218 distribution and development of handedness for manual gestures in captive chimpanzees
1219 (*Pan troglodytes*). Psychological Science 16, 487–493.

1220 Höppner, H., Grosse-Dunker, M., Stillfried, G., Bayer, J., van der Smagt, P., 2017. Key insights
1221 into hand biomechanics: human grip stiffness can be decoupled from force by cocontraction
1222 and predicted from electromyography. Frontiers in Neurorobotics 11, 1–17.

1223 Höppner, H., McIntyre, J., van der Smagt, P., 2013. Task dependency of grip stiffness—a study
1224 of human grip force and grip stiffness dependency during two different tasks with same grip
1225 forces. PLoS One 8, e80889.

1226 Hu, D., Howard, D., Ren, L., 2014. Biomechanical analysis of the human finger extensor
1227 mechanism during isometric pressing. PLoS One 9, e94533.

1228 Hunt, K.D., 1991. Mechanical implications of chimpanzee positional behavior. American Journal
1229 of Physical Anthropology 86, 521–536.

1230 Iwasaki, N., Genda, E., Minami, A., Kaneda, K., Chao, E.Y.S., 1998. Force transmission through
1231 the wrist joint in Kienböck's disease: A two-dimensional theoretical study. Journal of Hand
1232 Surgery 23, 415–424.

1233 Jones, F.W., 1916. Arboreal Man. Longmans Green and Co., London.

1234 Joshi, A.A., Leahy, R.M., Badawi, R.D., Chaudhari, A.J., 2016. Registration-based morphometry
1235 for shape analysis of the bones of the human wrist. IEEE Transactions on Medical Imaging 35,
1236 416–426.

1237 Karakostis, F.A., Hotz, G., Scherf, H., Wahl, J., Harvati, K., 2017. Occupational manual activity is
1238 reflected on the patterns among hand entheses. American Journal of Physical Anthropology
1239 164, 30–40.

1240 Karakostis, F.A., Lorenzo, C., 2016. Morphometric patterns among the 3D surface areas of
1241 human hand entheses. American Journal of Physical Anthropology 160, 694–707.

1242 Kargov, A., Pylatiuk, C., Martin, J., Schulz, S., Doderlein, L., 2004. A comparison of the grip force
1243 distribution in natural hands and in prosthetic hands. Disability and Rehabilitation 26, 705–
1244 711.

1245 Keaveny, T.M., Morgan, E.F., Niebur, G.L., Yeh, O.C., 2001. Biomechanics of trabecular bone.
1246 Annual Review of Biomedical Engineering 3, 307–333.

1247 Kerkhof, F.D., Brugman, E., D'Agostino, P., Dourthe, B., van Lenthe, G.H., Stockmans, F., Jonkers,
1248 I., Vereecke, E.E., 2016. Quantifying thumb opposition kinematics using dynamic computed
1249 tomography. Journal of Biomechanics 49, 1994–1999.

1250 Key, A.J., 2016. Manual loading distribution during carrying behaviors: implications for the
1251 evolution of the hominin hand. PLoS One 11, e0163801.

1252 Key, A.J., Dunmore, C.J., 2015. The evolution of the hominin thumb and the influence exerted
1253 by the non-dominant hand during stone tool production. Journal of Human Evolution 78, 60–
1254 69.

1255 Key, A., Dunmore, C.J., Hatala, K.G., Williams-Hatala, E.M., 2017. Flake morphology as a record
1256 of manual pressure during stone tool production. Journal of Archaeological Science: Reports
1257 12, 43–53.

1258 Key, A.J.M., Lycett, S.J., 2011. Technology based evolution? A biometric test of the effects of
1259 handsize versus tool form on efficiency in an experimental cutting task. Journal of
1260 Archaeological Science 38, 1663–1670.

1261 Key, A.J.M., Lycett, S.J., 2016. Investigating interrelationships between Lower Palaeolithic stone
1262 tool effectiveness and tool user biometric variation: implications for technological and
1263 evolutionary changes. Archaeological and Anthropological Sciences.
1264 https://doi.org/10.1007/s12520-016-0433-x

1265 Kivell, T.L., Barros, A.P., Smaers, J.B., 2013. Different evolutionary pathways underlie the
1266 morphology of wrist bones in hominoids. BMC Evolutionary Biololgy 13, 229.

1267 Kivell, T.L., Deane, A.S., Tocheri, M.W., Orr, C.M., Schmid, P., Hawks, J., Berger, L.R., Churchill,
1268 S.E., 2015. The hand of *Homo naledi*. Nature Communications 6, 8431.

1269 Kivell, T.L., Kibii, J.M., Churchill, S.E., Schmid, P., Berger, L.R., 2011a. Australopithecus sediba
1270 hand demonstrates mosaic evolution of locomotor and manipulative abilities. Science 333,
1271 1411–1417.

1272 Kivell, T.L., Skinner, M.M., Lazenby, R., Hublin, J.J., 2011b. Methodological considerations for
1273 analyzing trabecular architecture: an example from the primate hand. Journal of Anatomy
1274 218, 209–225.

1275 Ladd, A.L., Crisco, J.J., Hagert, E., Rose, J., Weiss, A.P., 2014. The 2014 ABJS Nicolas Andry
1276 Award: The puzzle of the thumb: mobility, stability, and demands in opposition. Clinical
1277 Orthopaedics and Relatated Research 472, 3605–3622.

1278 Lambers, F.M., Koch, K., Kuhn, G., Ruffoni, D., Weigt, C., Schulte, F.A., Muller, R., 2013.
1279 Trabecular bone adapts to long-term cyclic loading by increasing stiffness and normalization
1280 of dynamic morphometric rates. Bone 55, 325–334.

1281 Landsmeer, J.M., 1955. Anatomical and functional investigations on the articulation of the
1282 human fingers. Acta Anatomica Supplementum 25, 1–69.

1283 Landsmeer, J.M., 1962. Power grip and precision handling. Annals of the Rheumatic Diseases
1284 21, 164–170.

1285 Landsmeer, J.M., Long, C., 1965. The mechanism of finger control, based on electromyograms
1286 and location analysis. Acta Anatomica 60, 330–347.

1287 Lanyon, L., Rubin, C., 1985. Functional adaptation in skeletal structures. In: Hildebrand, M.,
1288 Bramble, D.M., Liem, K.F., Wake, D.B. (Eds.), Functional Vertebrate Morphology. Belknap,
1289 Cambridge, pp. 1–25.

1290 Latypova, A., Pioletti, D.P., Terrier, A., 2017. Importance of trabecular anisotropy in finite
1291 element predictions of patellar strain after total knee arthroplasty. Medical Engineering and
1292 Physics 39, 102–105.

1293 Lazenby, R.A., Angus, S., Cooper, D.M., Hallgrimsson, B., 2008a. A three-dimensional
1294 microcomputed tomographic study of site-specific variation in trabecular microarchitecture
1295 in the human second metacarpal. Journal of Anatomy 213, 698–705.

1296 Lazenby, R.A., Cooper, D.M., Angus, S., Hallgrimsson, B., 2008b. Articular constraint,
1297 handedness, and directional asymmetry in the human second metacarpal. Journal of Human
1298 Evolution 54, 875–885.

1299 Lazenby, R.A., Skinner, M.M., Hublin, J.J., Boesch, C., 2011a. Metacarpal trabecular architecture
1300 variation in the chimpanzee (*Pan troglodytes*): Evidence for locomotion and tool-use?
1301 American Journal of Physical Anthropology 144, 215–225.

1302 Lazenby, R.A., Skinner, M.M., Kivell, T.L., Hublin, J.J., 2011b. Scaling VOI size in 3D muCT studies
1303 of trabecular bone: a test of the over-sampling hypothesis. American Journal of Physical
1304 Anthropology 144, 196–203.

1305 Lazic, S.E., 2010. The problem of pseudoreplication in neuroscientific studies: is it affecting your
1306 analysis? BMC Neuroscience 11, 5.

1307 Leakey, L.S., Tobias, P.V., Napier, J.R., 1964. A New Species of the Genus *Homo* from Olduvai
1308 Gorge. Nature 202, 7–9.

1309 Lee, A.T., Williams, A.A., Lee, J., Cheng, R., Lindsey, D.P., Ladd, A.L., 2013. Trapezium trabecular
1310 morphology in carpometacarpal arthritis. Journal of Hand Surgery 38, 309–315.

1311 Lemelin, P., Schmitt, D., 2016. On primitiveness, prehensility, and opposability of the primate
1312 hand: the contributions of Frederic Wood Jones and John Russell Napier. In: Kivell, T.L.,
1313 Lemelin, P., Richmond, B.G., Schmitt, D. (Eds.), The Evolution of the Primate Hand. Springer,
1314 New York, pp. 5–13.

1315 Leventhal, E.L., Moore, D.C., Akelman, E., Wolfe, S.W., Crisco, J.J., 2010. Carpal and forearm
1316 kinematics during a simulated hammering task. Journal of Hand Surgery 35, 1097–1104.

1317 Lewis, O.J., 1969. The hominoid wrist joint. American Journal of Physical Anthropology 30, 251–
1318 267.

1319 Liu, M.J., Xiong, C.H., Hu, D., 2016a. Assessing the manipulative potentials of monkeys, apes and
1320 humans from hand proportions: implications for hand evolution. Proceedings of the Royal
1321 Society B 283, 20161923.

1322 Liu, Y., Jiang, L., Yang, D., Liu, H., 2016b. Analysis of Hand and Wrist Postural Synergies in
1323 Tolerance Grasping of Various Objects. PLoS One 11, e0161772.

1324 Lorenzo, C., Arsuaga, J.L., Carretero, J.M., 1999. Hand and foot remains from the Gran Dolina
1325 Early Pleistocene site (Sierra de Atapuerca, Spain). Journal of Human Evolution 37, 501–522.

1326 Lorenzo, C., Pablos, A., Carretero, J.M., Huguet, R., Valverdú, J., Martinón-Torres, M., Arsuaga,
1327 J.L., Carbonell, E., Bermúdez de Castro, J.M., 2015. Early Pleistocene human hand phalanx
1328 from the Sima del Elefante (TE) cave site in Sierra de Atapuerca (Spain). Journal of Human
1329 Evolution 78, 114–121.

1330 Macintosh, A.A., Pinhasi, R., Stock, J.T., 2014. Divergence in male and female manipulative
1331 behaviors with the intensification of metallurgy in Central Europe. PLoS One 9, e112116.

1332 Macintosh, A.A., Pinhasi, R., Stock, J.T., 2017. Prehistoric women's manual labor exceeded that
1333 of athletes through the first 5500 years of farming in Central Europe. Science Advances 3,
1334 eaao3893.

1335 Majima, M., Horii, E., Matsuki, H., Hirata, H., Genda, E., 2008. Load transmission through the
1336 wrist in the extended position. Journal of Hand Surgery 33, 182–188.

1337 Maki, J., Trinkaus, E., 2011. Opponens pollicis mechanical effectiveness in neandertals and early
1338 modern humans. PaleoAnthropology 2011, 62–71.

1339 Maquer, G., Musy, S.N., Wandel, J., Gross, T., Zysset, P.K., 2015. Bone volume fraction and
1340 fabric anisotropy are better determinants of trabecular bone stiffness than other
1341 morphological variables. Journal of Bone and Mineral Research 30, 1000–1008.

1342 Marangoni, A., Belli, L.M., Caramelli, D., Jacopo, M.C., Zavattaro, M., Manzi, G., 2011. The Tierra
1343 del Fuego, its ancient inhabitants, and the collections of human skeletal remains in the
1344 Museums of Anthropology of Florence and Rome. Museological significance, past
1345 researches, perspectives. Museologia Scientifica 5, 88–96.

1346 Marchi, D., 2005. The cross-sectional geometry of the hand and foot bones of the hominoidea
1347 and its relationship to locomotor behavior. Journal of Human Evolution 49, 743–761.

1348 Marchi, D., Shaw, C.N., 2011. Variation in fibular robusticity reflects variation in mobility
1349 patterns. Journal of Human Evolution 61, 609–616.

1350 Márquez-Florez, K., Vergara-Amador, E., de Las Casas, E.B., Garzón-Alvarado, D.A., 2015.
1351 Theoretical distribution of load in the radius and ulna carpal joint. Computers in Biology and
1352 Medicine 60, 100–106.

1353 Marzke, M.W., 1983. Joint functions and grips of the *Australopithecus afarensis* hand, with
1354 special reference to the region of the capitate. Journal of Human Evolution 12, 197–211.

1355 Marzke, M.W., 1997. Precision grips, hand morphology, and tools. American Journal of Physical
1356 Anthropology 102, 91–110.

1357 Marzke, M.W., 2013. Tool making, hand morphology and fossil hominins. Philosophical
1358 Transactions of the Royal Society B 368, 20120414.

1359 Marzke, M.W., Marchant, L.F., McGrew, W.C., Reece, S.P., 2015. Grips and hand movements of
1360 chimpanzees during feeding in Mahale Mountains National Park, Tanzania. American Journal
1361 of Physical Anthropology 156, 317–326.

1362 Marzke, M.W., Tocheri, M.W., Steinberg, B., Femiani, J.D., Reece, S.P., Linscheid, R.L., Orr, C.M.,
1363 Marzke, R.F., 2010. Comparative 3D quantitative analyses of trapeziometacarpal joint
1364 surface curvatures among living catarrhines and fossil hominins. American Journal of
1365 Physical Anthropology 141, 38–51.

1366 Marzke, M.W., Toth, N., Schick, K., Reece, S., Steinberg, B., Hunt, K., Linscheid, R.L., An, K.N.,
1367 1998. EMG study of hand muscle recruitment during hard hammer percussion manufacture
1368 of Oldowan tools. American Journal of Physical Anthropology 105, 315–332.

1369 Marzke, M.W., Wullstein, K.L., 1996. Chimpanzee and human grips: A new classification with a
1370 focus on evolutionary morphology. International Journal of Primatology 17, 117–139.

1371 Marzke, M.W., Wullstein, K.L., Viegas, S.F., 1992. Evolution of the power ("squeeze") grip and
1372 its morphological correlates in hominids. American Journal of Physical Anthropology 89,
1373 283–298.

1374 Matarazzo, S.A., 2015. Trabecular architecture of the manual elements reflects locomotor
1375 patterns in primates. PLoS One 10, e0120436.

1376 Mittnik, A., Wang, C.C., Svoboda, J., Krause, J., 2016. A molecular approach to the sexing of the
1377 triple burial at the upper paleolithic site of Dolní Věstonice. PLoS One 11, e0163019.

1378 Moojen, T.M., Snel, J.G., Ritt, M.J., Kauer, J.M., Venema, H.W., Bos, K.E., 2002a. Three-
1379 dimensional carpal kinematics in vivo. Clinical Biomechanics 17, 506–514.

1380 Moojen, T.M., Snel, J.G., Ritt, M.J., Venema, H.W., Kauer, J.M., Bos, K.E., 2002b. Scaphoid
1381 kinematics in vivo. Journal of Hand Surgery 27, 1003–1010.

1382 Musgrave, J.H., 1971. How dextrous was neanderthal man? Nature 233, 538–541.

1383 Napier, J., 1962. Fossil hand bones from Olduvai Gorge. Nature 196, 409–411.

1384 Napier, J.R., 1956. The prehensile movements of the human hand. Journal of Bone and Joint
1385 Surgery, British Volume 38-B, 902–913.

1386 Napier, J.R., 1960. Studies of the hands of living primates. Proceedings of the Zoological Society
1387 of London 134, 647–657.

1388 Neufuss, J., Humle, T., Cremaschi, A., Kivell, T.L., 2017. Nut-cracking behavior in wild-born,
1389 rehabilitated bonobos (*Pan paniscus*): a comprehensive study of hand-preference, hand
1390 grips and efficiency. American Journal of Primatology 79, 1–16.

1391 Niewoehner, W.A., 2001. Behavioral inferences from the Skhul/Qafzeh early modern human
1392 hand remains. Proceedings of the National Academy of Sciences USA 98, 2979–2984.

1393 Niewoehner, W., 2006. Neanderthal hands in their proper perspective. In: Harvati, K., Harrison,
1394 T. (Eds.), Neanderthals Revisited: New Approaches and Perspectives, 2nd ed. Springer,
1395 Dordrecht, pp. 157–190.

1396 Niewoehner, W.A., Bergstrom, A., Eichele, D., Zuroff, M., Clark, J.T., 2003. Digital analysis:
1397 manual dexterity in Neanderthals. Nature 422, 395.

1398 Nufer, P., Goldhahn, J., Kohler, T., Kuhn, V., Muller, R., Herren, D.B., 2008. Microstructural
1399 adaptation in trapezial bone due to subluxation of the thumb. Journal of Orthopaedic
1400 Research 26, 208–216.

1401 Orr, C.M., 2017. Locomotor hand postures, carpal kinematics during wrist extension, and
1402 associated morphology in anthropoid primates. Anatomical Record 300, 382–401.

1403 Orr, C.M., 2018. Kinematics of the anthropoid os centrale and the functional consequences of
1404 scaphoid-centrale fusion in African apes and hominins. Journal of Human Evolution 114,
1405 102–117.

1406 Orr, C.M., Leventhal, E.L., Chivers, S.F., Marzke, M.W., Wolfe, S.W., Crisco, J.J., 2010. Studying
1407 primate carpal kinematics in three dimensions using a computed-tomography-based
1408 markerless registration method. Anatomical Record 293, 692–709.

1409 Ozcivici, E., Judex, S., 2014. Trabecular bone recovers from mechanical unloading primarily by
1410 restoring its mechanical function rather than its morphology. Bone 67, 122–129.

1411 Pahr, D.H., Zysset, P.K., 2009a. A comparison of enhanced continuum FE with micro FE models
1412 of human vertebral bodies. Journal of Biomechanics 42, 455–462.

1413 Pahr, D.H., Zysset, P.K., 2009b. From high-resolution CT data to finite element models:
1414 development of an integrated modular framework. Computer Methods in Biomechanics and
1415 Biomedical Engineering 12, 45–57.

1416 Pahr, D.H., Zysset, P.K., 2016. Finite element-based mechanical assessment of bone quality on
1417 the basis of in vivo images. Current Osteoporosis Reports 14, 374–385.

1418 Paoli, G., Borgognini Tarli, S.M., Klir, P., Strouhal, E., Tofanelli, S., Del Santo Valli, M.T.,
1419 Pavelcova, B., 1993. Paleoserology of the Christian population at Sayala (Lower Nubia): an
1420 evaluation of the reliability of the results. American Journal of Physical Anthropology 92,
1421 263–272.

Pataky, T.C., Slota, G.P., Latash, M.L., Zatsiorsky, V.M., 2012. Radial force distribution changes associated with tangential force production in cylindrical grasping, and the importance of anatomical registration. Journal of Biomechanics 45, 218–224.

Patel, B.A., Carlson, K.J., 2007. Bone density spatial patterns in the distal radius reflect habitual hand postures adopted by quadrupedal primates. Journal of Human Evolution 52, 130–141.

Pearson, O.M., Sparacello, V.S., 2017. Behavioral differences between near eastern neanderthals and the early modern humans from Skhul and Qafzeh: an assessment based on comparative samples of Holocene humans. In: Marom, A., Hovers, E. (Eds.), Human Paleontology and Prehistory. Springer International Publishing, Cham, pp. 175–186.

Perchalski, B., Placke, A., Sukhdeo, S.M., Shaw, C.N., Gosman, J.H., Raichlen, D.A., Ryan, T.M., 2017. Asymmetry in the cortical and trabecular bone of the human humerus during development. Anatomical Record. https://doi.org/10.1002/ar.23705

Phillips, A.T.M., Villette, C.C., Modenese, L., 2015. Femoral bone mesoscale structural architecture prediction using musculoskeletal and finite element modelling. International Biomechanics 2, 43–61.

Polk, J.D., 2002. Adaptive and phylogenetic influences on musculoskeletal design in cercopithecine primates. Journal of Experimental Biology 205, 3399–3412.

Pontzer, H., Lieberman, D.E., Momin, E., Devlin, M.J., Polk, J.D., Hallgrimsson, B., Cooper, D.M., 2006. Trabecular bone in the bird knee responds with high sensitivity to changes in load orientation. Journal of Experimental Biology 209, 57–65.

1442 Poole, K.E., Treece, G.M., Mayhew, P.M., Vaculik, J., Dungl, P., Horak, M., Stepan, J.J., Gee, A.H.,
1443 2012. Cortical thickness mapping to identify focal osteoporosis in patients with hip fracture.
1444 PLoS One 7, e38466.

1445 Pouydebat, E., Gorce, P., Coppens, Y., Bels, V., 2009. Biomechanical study of grasping according
1446 to the volume of the object: human versus non-human primates. Journal of Biomechanics
1447 42, 266–272.

1448 Pouydebat, E., Fragaszy, D., Kivell, T.L., 2014. Grasping in primates: for feeding, moving and
1449 human specificities. Bulletins et Mémoires de la Société d'Anthropologie de Paris, 26, 129–
1450 133.

1451 Pouydebat, E., Reghem, E., Borel, A., Gorce, P., 2011. Diversity of grip in adults and young
1452 humans and chimpanzees (*Pan troglodytes*). Behavioural Brain Research 218, 21–28.

1453 Proffitt, T., Luncz, L.V., Falotico, T., Ottoni, E.B., de la Torre, I., Haslam, M., 2016. Wild monkeys
1454 flake stone tools. Nature 539, 85–88.

1455 Putt, S.S., Wijeakumar, S., Franciscus, R.G., Spencer, J.P., 2017. The functional brain networks
1456 that underlie Early Stone Age tool manufacture. Nature Human Behaviour 1, 0102.

1457 Python 3.6, 2017. Python programming language. Python Software Foundation, Beaverton.

1458 Qiu, D., Kamper, D.G., 2014. Orthopaedic applications of a validated force-based biomechanical
1459 model of the index finger. In: 36th Annual International Conference of the IEEE Engineering
1460 in Medicine and Biology Society. IEEE, Chicago, pp. 4013–4016.

R Core Team, 2017. R: A language and environment for statistical computing. R Foundation for Statistical Computing, Vienna.

Rabey, K.N., Green, D.J., Taylor, A.B., Begun, D.R., Richmond, B.G., McFarlin, S.C., 2015. Locomotor activity influences muscle architecture and bone growth but not muscle attachment site morphology. Journal of Human Evolution 78, 91–102.

Rafferty, K.L., Ruff, C.B., 1994. Articular structure and function in *Hylobates*, *Colobus*, and *Papio*. American Journal of Physical Anthropology 94, 395–408.

Rainbow, M.J., Kamal, R.N., Leventhal, E., Akelman, E., Moore, D.C., Wolfe, S.W., Crisco, J.J., 2013. In vivo kinematics of the scaphoid, lunate, capitate, and third metacarpal in extreme wrist flexion and extension. Journal of Hand Surgery 38, 278–288.

Rainbow, M.J., Kamal, R.N., Moore, D.C., Akelman, E., Wolfe, S.W., Crisco, J.J., 2015. Subject-specific carpal ligament elongation in extreme positions, grip, and the dart thrower's motion. Journal of Biomechanical Engineering 137, 111006.

Rainbow, M.J., Wolff, A.L., Crisco, J.J., Wolfe, S.W., 2016. Functional kinematics of the wrist. Journal of Hand Surgery Europe 41, 7–21.

Reina, N., Cavaignac, E., Trousdale, W.H., Laffosse, J.M., Braga, J., 2017. Laterality and grip strength influence hand bone micro-architecture in modern humans, an HRpQCT study. Journal of Anatomy 230, 796–804.

Reznikov, N., Chase, H., Brumfeld, V., Shahar, R., Weiner, S., 2015. The 3D structure of the collagen fibril network in human trabecular bone: relation to trabecular organization. Bone 71, 189–195.

1482 Reznikov, N., Phillips, C., Cooke, M., Garbout, A., Ahmed, F., Stevens, M.M., 2017. Functional
1483 adaptation of the calcaneus in historical foot binding. Journal of Bone and Mineral Research
1484 32, 1915–1925.

1485 Rhodes, J.A., Knusel, C.J., 2005. Activity-related skeletal change in medieval humeri: cross-
1486 sectional and architectural alterations. American Journal of Physical Anthropology 128, 536–
1487 546.

1488 Ricklan, D.E., 1987. Functional anatomy of the hand of *Australopithecus africanus*. Journal of
1489 Human Evolution 16, 643–664.

1490 Ritter, Z., Belavy, D., Baumann, W.W., Felsenberg, D., 2017. In vivo bone modeling rates
1491 determination and compressive stiffness variations before, during 60 days bed rest and two
1492 years follow up: A micro-FE-analysis from HR-pQCT measurements of the berlin Bed Rest
1493 Study-2. Acta Astronautica 132, 67–77.

1494 Roberts, T.J., Konow, N., 2013. How tendons buffer energy dissipation by muscle. Exercise and
1495 Sport Sciences Reviews 41, 186–193.

1496 Rolian, C., 2016. The role of genes and development in the evolution of the primate hand. In:
1497 Kivell, T.L., Lemelin, P., Richmond, B.G., Schmitt, D. (Eds.), The Evolution of the Primate
1498 Hand. Springer, New York, pp. 101–130.

1499 Rolian, C., Lieberman, D.E., Hallgrimsson, B., 2010. The coevolution of human hands and feet.
1500 Evolution 64, 1558–1568.

1501 Rolian, C., Lieberman, D.E., Zermeno, J.P., 2011. Hand biomechanics during simulated stone
1502 tool use. Journal of Human Evolution 61, 26–41.

1503 Ruff, C.B., 2002. Long bone articular and diaphyseal structure in old world monkeys and apes. I:
1504 locomotor effects. American Journal of Physical Anthropology 119, 305–342.

1505 Ruff, C., Holt, B., Trinkaus, E., 2006. Who's afraid of the big bad Wolff?: "Wolff's law" and bone
1506 functional adaptation. American Journal of Physical Anthropology 129, 484-498.

1507 Ryan, T.M., Ketcham, R.A., 2002. Femoral head trabecular bone structure in two omomyid
1508 primates. Journal of Human Evolution 43, 241–263.

1509 Ryan, T.M., Shaw, C.N., 2012. Unique suites of trabecular bone features characterize locomotor
1510 behavior in human and non-human anthropoid primates. PLoS One 7, e41037.

1511 Ryan, T.M., Shaw, C.N., 2013. Trabecular bone microstructure scales allometrically in the
1512 primate humerus and femur. Proceedings of the Royal Society B: Biological Sciences 280,
1513 20130172.

1514 Ryan, T.M., Shaw, C.N., 2015. Gracility of the modern *Homo sapiens* skeleton is the result of
1515 decreased biomechanical loading. Proceedings of the National Academy of Sciences of the
1516 United States of America 112, 372–377.

1517 Ryan, T.M., Raichlen, D.A., Gosman, J.H., 2017. Structural and mechanical changes in trabecular
1518 bone during early development in the human femur and humerus. In: Percival, C.J.,
1519 Richtsmeier, J.T. (Eds.), Building Bones: Bone Formation and Development in Anthropology.
1520 Cambridge University Press, Cambridge, pp. 281–302.

1521 Saffar, R.A.A., 2016. Quantification of variable palmar ligaments around the triquetrum-hamate
1522 joint determined by lunate type. Ph.D. Dissertation, University of Glasgow.

1523 Scherf, H., Tilgner, R., 2009. A new high-resolution computed tomography (CT) segmentation
1524 method for trabecular bone architectural analysis. American Journal of Physical
1525 Anthropology 140, 39–51.

1526 Scherf, H., Wahl, J., Hublin, J.J., Harvati, K., 2016. Patterns of activity adaptation in humeral
1527 trabecular bone in Neolithic humans and present-day people. American Journal of Physical
1528 Anthropology 159, 106–115.

1529 Schilling, A.M., Tofanelli, S., Hublin, J.J., Kivell, T.L., 2014. Trabecular bone structure in the
1530 primate wrist. Journal of Morphology 275, 572–585.

1531 Schlecht, S.H., Bigelow, E.M., Jepsen, K.J., 2014. Mapping the natural variation in whole bone
1532 stiffness and strength across skeletal sites. Bone 67, 15–22.

1533 Schmid, P., Berger, L.R., 1997. Middle Pleistocene hominid carpal proximal phalanx from the
1534 Gladysvale site, South Africa. South African Journal of Science 93, 430–431.

1535 Schneider, M.T.Y., Zhang, J., Crisco, J.J., Weiss, A.C., Ladd, A.L., Mithraratne, K., Nielsen, P.,
1536 Besier, T., 2017. Trapeziometacarpal joint contact varies between men and women during
1537 three isometric functional tasks. Medical Engineering & Physics 50, 43–49.

1538 Schulte, F.A., Lambers, F.M., Kuhn, G., Muller, R., 2011. In vivo micro-computed tomography
1539 allows direct three-dimensional quantification of both bone formation and bone resorption
1540 parameters using time-lapsed imaging. Bone 48, 433–442.

1541 Schulte, F.A., Ruffoni, D., Lambers, F.M., Christen, D., Webster, D.J., Kuhn, G., Muller, R., 2013.
1542 Local mechanical stimuli regulate bone formation and resorption in mice at the tissue level.
1543 PLoS One 8, e62172.

1544 Shaw, C.N., Hofmann, C.L., Petraglia, M.D., Stock, J.T., Gottschall, J.S., 2012. Neandertal humeri
1545 may reflect adaptation to scraping tasks, but not spear thrusting. PLoS One 7, e40349.

1546 Schwarcz, H.P., Grün, R., Vandermeersch, B., Bar-Yosef, O., Valladas, H., Tchernov, E., 1988. ESR
1547 dates for the hominid burial site of Qafzeh in Israel. Journal of Human Evolution 17, 733–
1548 737.

1549 Schwiedrzik, J., Gross, T., Bina, M., Pretterklieber, M., Zysset, P., Pahr, D., 2016. Experimental
1550 validation of a nonlinear muFE model based on cohesive-frictional plasticity for trabecular
1551 bone. International Journal for Numerical Methods in Biomedical Engineering 32, e02739.

1552 Shrewsbury, M.M., Marzke, M.W., Linscheid, R.L., Reece, S.P., 2003. Comparative morphology
1553 of the pollical distal phalanx. American Journal of Physical Anthropology 121, 30–47.

1554 Singh, M., Nagrath, A.R., Maini, P.S., 1970. Changes in trabecular pattern of the upper end of
1555 the femur as an index of osteoporosis. Journal of Bone and Joint Surgery 52, 457–467.

1556 Skinner, M.M., Stephens, N.B., Tsegai, Z.J., Foote, A.C., Nguyen, N.H., Gross, T., Pahr, D.H.,
1557 Hublin, J.J., Kivell, T.L., 2015a. Human-like hand use in *Australopithecus africanus*. Science
1558 347, 395–399.

1559 Skinner, M.M., Stephens, N.B., Tsegai, Z.J., Foote, A.C., Nguyen, N.H., Gross, T., Pahr, D.H.,
1560 Hublin, J.J., Kivell, T.L., 2015b. Response to comment on “Human-like hand use in
1561 *Australopithecus africanus*”. Science 348, 1101.

1562 Sládek, V., Hora, M., Farkašová, K., Rocek, T.R., 2016. Impact of grinding technology on bilateral
1563 asymmetry in muscle activity of the upper limb. Journal of Archaeological Science 72, 142–
1564 156.

1565 Sládek, V., Trinkaus, E., Hillson, S.W., Holliday, T.W., 2000. The People of the Pavlovian: Skeletal
1566 Catalogue and Osteometrics of the Gravettian Fossil Hominids from Dolní Věstonice and
1567 Pavlov. Academy of Sciences of the Czech Republic, Institute of Archaeology, Brno, Dolní
1568 Věstonice.

1569 Smith, L.M., Bigelow, E.M., Nolan, B.T., Faillace, M.E., Nadeau, J.H., Jepsen, K.J., 2014. Genetic
1570 perturbations that impair functional trait interactions lead to reduced bone strength and
1571 increased fragility in mice. Bone 67, 130–138.

1572 Sparacello, V., Pettitt, P.B., Roberts, C., 2015. Funerary dynamics of an Epipalaeolithic cemetery:
1573 a new database on Arene Candide skeletal remains. Proceedings of the European Society for
1574 the Study of Human Evolution 4, 209.

1575 Stephens, N.B., Kivell, T.L., Pahr, D.H., Hublin, J.J., Skinner, M.M., 2015. Visualising trabecular
1576 bone architecture and distribution in the human hand: variation, consistency, and
1577 implications for reconstructing behaviour. Proceedings of the European Society for the Study
1578 of Human Evolution 4, 211.

1579 Stephens, N.B., Kivell, T.L., Gross, T., Pahr, D.H., Lazenby, R.A., Hublin, J.J., Hershkovitz, I.,
1580 Skinner, M.M., 2016a. Trabecular architecture in the thumb of *Pan* and *Homo*: implications
1581 for investigating hand use, loading, and hand preference in the fossil record. American
1582 Journal of Physical Anthropology 161, 603–619.

1583 Stephens, N.B., Kivell, T.L., Pahr, D.H., Gee, A.H., Treece, G.M., Hublin, J.J., Skinner, M.M.,
1584 2016b. Signals of loading and function in the human hand: a multi-method analysis of the

external cortical and internal trabecular bone of the metacarpals. American Journal of Physical Anthropology 159 S62, 302–303.

Stieglitz, J., Trumble, B.C., Kaplan, H., Gurven, M., 2017. Horticultural activity predicts later localized limb status in a contemporary pre-industrial sample. American Journal of Physical Anthropology 163, 425–436.

Stock, J.T., 2006. Hunter-gatherer postcranial robusticity relative to patterns of mobility, climatic adaptation, and selection for tissue economy. American Journal of Physical Anthropology 131, 194–204.

Stock, J.T., Shirley, M.K., Sarringhaus, L.A., Davies, T.G., Shaw, C.N., 2013. Skeletal evidence for variable patterns of handedness in chimpanzees, human hunter-gatherers, and recent British populations. Annals of the New York Academy of Sciences 1288, 86–99.

Stratford, D., Heaton, J.L., Pickering, T.R., Caruana, M.V., Shadrach, K., 2016. First hominin fossils from Milner Hall, Sterkfontein, South Africa. Journal of Human Evolution 91, 167–173.

Strauss, A., Oliveira, R.E., Bernardo, D.V., Salazar-Garcia, D.C., Talamo, S., Jaouen, K., Hubbe, M., Black, S., Wilkinson, C., Richards, M.P., Araujo, A.G., Kipnis, R., Neves, W.A., 2015. The oldest case of decapitation in the new world (Lapa do Santo, east-central Brazil). PLoS One 10, e0137456.

Strouhal, E., Jungwirth, J., 1979. Paleogenetics of the late Roman-early Byzantine cemeteries at Sayala, Egyptian Nubia. Journal of Human Evolution 8, 699–703.

Su, A., Carlson, K.J., 2017. Comparative analysis of trabecular bone structure and orientation in South African hominin tali. Journal of Human Evolution 106, 1–18.

1606 Su, A., Wallace, I.J., Nakatsukasa, M., 2013. Trabecular bone anisotropy and orientation in an
1607 early Pleistocene hominin talus from East Turkana, Kenya. Journal of Human Evolution 64,
1608 667–677.

1609 Sugiyama, T., Price, J.S., Lanyon, L.E., 2010. Functional adaptation to mechanical loading in both
1610 cortical and cancellous bone is controlled locally and is confined to the loaded bones. Bone
1611 46, 314–321.

1612 Susman, R.L., 1979. Comparative and functional morphology of hominoid fingers. American
1613 Journal of Physical Anthropology 50, 215–236.

1614 Susman, R.L., 1991. Who made the oldowan tools? Fossil evidence for tool behavior in Plio-
1615 Pleistocene hominids. Journal of Anthropological Research 47, 129–151.

1616 Susman, R.L., 1994. Fossil evidence for early hominid tool use. Science 265, 1570–1573.

1617 Susman, R.L., 1998. Hand function and tool behavior in early hominids. Journal of Human
1618 Evolution 35, 23–46.

1619 Sylvester, A.D., Terhune, C.E., 2017. Trabecular mapping: Leveraging geometric morphometrics
1620 for analyses of trabecular structure. American Journal of Physical Anthropology 163, 553–
1621 569.

1622 Synek, A., Pahr, D.H., 2016. The effect of the extensor mechanism on maximum isometric
1623 fingertip forces: A numerical study on the index finger. Journal of Biomechanics 49, 3423–
1624 3429.

1625 Taghizadeh, E., Chandran, V., Reyes, M., Zysset, P., Buchler, P., 2017. Statistical analysis of the
1626 inter-individual variations of the bone shape, volume fraction and fabric and their
1627 correlations in the proximal femur. Bone 103, 252–261.

1628 Tocheri, M.W., Marzke, M.W., Liu, D., Bae, M., Jones, G.P., Williams, R.C., Razdan, A., 2003.
1629 Functional capabilities of modern and fossil hominid hands: three-dimensional analysis of
1630 trapezia. American Journal of Physical Anthropology 122, 101–112.

1631 Tocheri, M.W., Orr, C.M., Jacofsky, M.C., Marzke, M.W., 2008. The evolutionary history of the
1632 hominin hand since the last common ancestor of *Pan* and *Homo*. Journal of Anatomy 212,
1633 544–562.

1634 Tocheri, M.W., Razdan, A., Williams, R.C., Marzke, M.W., 2005. A 3D quantitative comparison of
1635 trapezium and trapezoid relative articular and nonarticular surface areas in modern humans
1636 and great apes. Journal of Human Evolution 49, 570–586.

1637 Tommasini, S.M., Hu, B., Nadeau, J.H., Jepsen, K.J., 2009. Phenotypic integration among
1638 trabecular and cortical bone traits establishes mechanical functionality of inbred mouse
1639 vertebrae. Journal of Bone and Mineral Research 24, 606–620.

1640 Trinkaus, E., 1989. Olduvai Hominid 7 trapezial metacarpal 1 articular morphology: contrasts
1641 with recent humans. American Journal of Physical Anthropology 80, 411–416.

1642 Trinkaus, E., Churchill, S.E., Ruff, C.B., 1994. Postcranial robusticity in Homo. II: Humeral
1643 bilateral asymmetry and bone plasticity. American Journal of Physical Anthropology 93, 1–
1644 34.

1645 Trinkaus, E., 2016. The evolution of the hand in Pleistocene *Homo*. In: Kivell, T.L., Lemelin, P.,
1646 Richmond, B.G., Schmitt, D. (Eds.), The Evolution of the Primate Hand. Springer, New York,
1647 pp. 545–571.

1648 Trinkaus, E., Formicola, V., Svoboda, J., Hillson, S.W., Holliday, T.W., 2001. Dolní Věstonice 15:
1649 pathology and persistence in the Pavlovian. Journal of Archaeological Science 28, 1291–
1650 1308.

1651 Tsegai, Z.J., Kivell, T.L., Gross, T., Nguyen, N.H., Pahr, D.H., Smaers, J.B., Skinner, M.M., 2013.
1652 Trabecular bone structure correlates with hand posture and use in hominoids. PLoS One 8,
1653 e78781.

1654 Tsegai, Z.J., Stephens, N.B., Treece, G.M., Skinner, M.M., Kivell, T.L., Gee, A.H., 2017. Cortical
1655 bone mapping: an application to hand and foot bones in hominoids. Comptes Rendus Palevol
1656 16, 690–701.

1657 Tsegai, Z.J., Skinner, M.M., Pahr, D.H., Hublin, J.-J., Kivell, T.L., 2018. Systemic patterns of
1658 trabecular bone across the human and chimpanzee skeleton. Journal of Anatomy.
1659 https://doi.org/10.1111/joa.12776

1660 Varga, P., Schefzig, P., Unger, E., Mayr, W., Zysset, P.K., Erhart, J., 2013. Finite element based
1661 estimation of contact areas and pressures of the human scaphoid in various functional
1662 positions of the hand. Journal of Biomechanics 46, 984–990.

1663 Venkataraman, V.V., Rolian, C., Gordon, A.D., Patel, B.A., 2013. A resampling approach and
1664 implications for estimating the phalangeal index from unassociated hand bones in fossil
1665 primates. American Journal of Physical Anthropology 151, 280–289.

1666 Vereecke, E.E., Wunderlich, R.E., 2016. Experimental research on hand use and function in
1667 primates. In: Kivell, T.L., Lemelin, P., Richmond, B.G., Schmitt, D. (Eds.), The Evolution of the
1668 Primate Hand. Springer, New York, pp. 259–284.

1669 Vergara, M., Sancho-Bru, J.L., Gracia-Ibáñez, V., Pérez-González, A., 2014. An introductory study
1670 of common grasps used by adults during performance of activities of daily living. Journal of
1671 Hand Therapy 27, 225–233.

1672 Viaro, R., Tia, B., Coude, G., Canto, R., Oliynyk, A., Salmas, P., Masia, L., Sandini, G., Fadiga, L.,
1673 2017. Finger pressure adjustments to various object configurations during precision grip in
1674 humans and monkeys. European Journal of Neuroscience 45, 1473–1484.

1675 Vickerton, P., Jarvis, J.C., Gallagher, J.A., Akhtar, R., Sutherland, H., Jeffery, N., 2014.
1676 Morphological and histological adaptation of muscle and bone to loading induced by
1677 repetitive activation of muscle. Proceedings of the Royal Society B 281, 20140786.

1678 Visalberghi, E., Addessi, E., Truppa, V., Spagnoletti, N., Ottoni, E., Izar, P., Fragaszy, D., 2009.
1679 Selection of effective stone tools by wild bearded capuchin monkeys. Current Biology 19,
1680 213–217.

1681 Vlček, E., 1975. Morphology of the first metacarpal of neandertal individuals from the Crimea.
1682 Bulletins et Mémoires de la Société d'Anthropologie de Paris 2, 257–276.

1683 Wallace, I.J., Middleton, K.M., Lublinsky, S., Kelly, S.A., Judex, S., Garland, T. Jr., Demes, B.,
1684 2010. Functional significance of genetic variation underlying limb bone diaphyseal structure.
1685 American Journal of Physical Anthropology 143, 21–30.

1686 Wallace, I.J., Judex, S., Demes, B., 2015a. Effects of load-bearing exercise on skeletal structure
1687 and mechanics differ between outbred samples of mice. Bone 72, 1–8.

1688 Wallace, I.J., Pagnotti, G.M., Rubin-Sigler, J., Naeher, M., Copes, L.E., Judex, S., Rubin, C.T.,
1689 Demes, B., 2015b. Focal enhancement of the skeleton to exercise correlates with
1690 responsivity of bone marrow mesenchymal stem cells rather than peak external forces.
1691 Journal of Experimental Biology 218, 3002–3009.

1692 Wallace, I.J., Demes, B., Judex, S., 2017a. Ontogenetic and genetic influences on bone's
1693 responsiveness to mechanical signals. In: Percival, C.J., Richtsmeier, J.T. (Eds.), Building
1694 Bones: Bone Formation and Development in Anthropology. Cambridge University Press,
1695 Cambridge, pp. 233–253.

1696 Wallace, I.J., Winchester, J.M., Su, A., Boyer, D.M., Konow, N., 2017b. Physical activity alters
1697 limb bone structure but not entheseal morphology. Journal of Human Evolution 107, 14–18.

1698 Ward, C.V., Tocheri, M.W., Plavcan, J.M., Brown, F.H., Manthi, F.K., 2014. Early Pleistocene third
1699 metacarpal from Kenya and the evolution of modern human-like hand morphology.
1700 Proceedings of the National Academy of Sciences USA 111, 121–124.

1701 Washburn, S.L., 1960. Tools and human evolution. Scientific American 203, 63–75.

1702 Waskom, M., Botvinnik, O., O'Kane, D., Hobson, P., Lukauskas, S., Gemperline, D.C., Augspurger,
1703 T., Halchenko, Y., Cole, J.B., Warmenhoven, J., Ruiter, J. de, Pye, C., Hoyer, S., Vanderplas, J.,
1704 Villalba, S., Kunter, G., Quintero, E., Bachant, P., Martin, M., Meyer, K., Miles, A., Ram, Y.,
1705 Yarkoni, T., Williams, M.L., Evans, C., Fitzgerald, C., Brian, Fonnesbeck, C., Lee, A., Qalieh, A.,

2017. Seaborn: statistical data visualization v0.8.0. Zenodo. https://doi.org//10.5281/zenodo.883859.

Whiten, A., Goodall, J., McGrew, W.C., Nishida, T., Reynolds, V., Sugiyama, Y., Tutin, C.E., Wrangham, R.W., Boesch, C., 1999. Cultures in chimpanzees. Nature 399, 682–685.

Williams, E.M., Gordon, A.D., Richmond, B.G., 2010. Upper limb kinematics and the role of the wrist during stone tool production. American Journal of Physical Anthropology 143, 134–145.

Williams, E.M., Gordon, A.D., Richmond, B.G., 2012. Hand pressure distribution during Oldowan stone tool production. Journal of Human Evolution 62, 520–532.

Williams, E.M., Gordon, A.D., Richmond, B.G., 2014. Biomechanical strategies for accuracy and force generation during stone tool production. Journal of Human Evolution 72, 52–63.

Williams-Hatala, E.M., Hatala, K.G., Gordon, M., Kasper, M., Kivell, T.L., 2017. The biomechanics of stone tool behaviors and implications for the evolution of the human hand. American Journal of Physical Anthropology 162, 411.

Wong, A.L., sMeals, C.G., Ruff, C.B., 2017. Computed tomographic analysis of the internal structure of the metacarpals and its impliscations for hand use, pathology, and surgical intervention. Anatomical Science International. https://doi.org/10.1007/s12565-017-0400-3.

Wood, B., 2014. Human evolution: fifty years after *Homo habilis*. Nature 508, 31–33.

Wu, J.Z., Sinsel, E.W., Zhao, K.D., An, K.N., Buczek, F.L., 2015. Analysis of the constraint joint loading in the thumb during pipetting. Journal of Biomechanical Engineering 137, 084501.

Yang, H., Embry, R.E., Main, R.P., 2017. Effects of loading duration and short rest insertion on cancellous and cortical bone adaptation in the mouse tibia. PLoS One 12, e0169519.

Young, R.W., 2003. Evolution of the human hand: the role of throwing and clubbing. Journal of Anatomy 202, 165–174.

Zeininger, A., Richmond, B.G., Hartman, G., 2011. Metacarpal head biomechanics: a comparative backscattered electron image analysis of trabecular bone mineral density in *Pan troglodytes*, *Pongo pygmaeus*, and *Homo sapiens*. Journal of Human Evolution 60, 703–710.

Zlatev, J., 2008. From proto-mimesis to language: evidence from primatology and social neuroscience. Journal of Physiology-Paris 102, 137–151.

Zysset, P.K., 2003. A review of morphology-elasticity relationships in human trabecular bone: theories and experiments. Journal of Biomechanics 36, 1469–1485.

Figure captions

Figure 1. Depiction of the linear mixed effect model setups in the study. Type 1 compares the segments (carpals, head/bases from the rays II–V), type 2 the regions of the metacarpals (head/base dorsoradial, dorsoulnar, palmoradial, palmoulnar), and type 3 the regions of the phalanges (head/base ulnar and radial). For each model type, 'subtype a' contains data from all the bones of the hand and 'subtype b' contains all data from the bones of the thumb. Bones are colored to help illustrate the different functional groups used in the linear models: hamatotrqiuetral (dark pink), capitotrapezoid (light pink), scapholunate (red-orange), thumb

group (purple), ray II (green), ray III (teal), ray IV (yellow), and ray V (orange). See text for a more detailed description.

Figure 2. Comparison of post-Neolithic and forager mean segment values. Values of BV/TV, E, and DA are all mapped onto right hands. Here the differences in the carpals and the heads of the phalanges are most obvious for BV/TV and E. Also note the extremely low DA in the carpals of the forager sample. The data pictured here pertains to model type 1.

Figure 3. Comparison of post-Neolithic and forager average Tb.Th (mm) and Tb.Sp (mm) by bone segment. Here the Tb.Sp is nearly identical between the two, with the Tb.Th differing in the carpals, metacarpal bases, and the heads of the phalanges.

Figure 4. Violin plots of each carpal bone for BV/TV, E, and DA, which show each individual value (horizontal black bars, with width defined by counts per bin) as well as the distribution by group (outer curve, defined by width multiplied by kernel of 2 standard deviations). The post-Neolithic sample is indicated by the lighter shades to the left of the vertical mid-bar, while the forager sample is indicated by darker shades to the right. Note the bimodal distribution for DA with some being very close to 0, which indicates isotropic organization. This distribution and range is the cause for the large standard deviations found in Table 3.

Figure 5. Metacarpal regional variation for the post-Neolithic and forager samples. Values of BV/TV, E, and DA are mapped onto right hands. The darkened areas in the palmar view represent the respective head/base segments. Here BV/TV and E both show a tendency for the heads to have higher relative values in the palmar/palmar-ulnar Mc2–Mc5 and palmar-radial

Mc1. Also note the variation in DA between the two samples. The data pictured here pertains to model type 2.

Figure 6. Phalangeal regional variation for the post-Neolithic and forager samples. Values of BV/TV, E, and DA are mapped onto rights hands in palmar view. Here there is little variation between the ulnar and radial regions for BV/TV and E, whereas DA varies more. Data pictured here pertains to model type 3.

Figure 7. Palmar (A) and dorsal (B) views of the average site-specific BV/TV for the post-Neolithic and forager samples. While both distributions are generally similar in the high value concentrations along the metacarpal and phalangeal head/ bases, the values for the forager sample are generally higher with the carpals and phalangeal heads being the most different.

Figure 8. Distal (A) and proximal (B) views of the average metacarpal site-specific BV/TV for the post-Neolithic and forager samples. Note how the relatively high site-specific BV/TV values in the palmoulnar Mc2–Mc5 heads and palmoradial Mc1 heads match the metacarpal regional variation for BV/TV and E (Fig. 5).

Figure 9. Proximal (A) and distal-palmar (B) view of average carpal site-specific BV/TV for the post-Neolithic and forager samples. Note the differences in high values concentrations along the radial surface of the triquetral, radiocarpal (proximal lunate and scaphoid), and midcarpal joints (distal lunate and scaphoid).

Figure 10. Ulnar-proximal (A) and radial-proximal (B) views of average hamate, capitate, and trapezoid site-specific BV/TV for the post-Neolithic and forager samples. Here both samples show high value concentrations along the capitate that correspond with those observed on the

lunate and scaphoid. Also note the correspondence of high value concentrations between the forager trapezoid and capitate that are not present in the post-Neolithic sample (B).

Figure 11. Cross-sectional views through the lunate, capitate, and ray III for post-Neolithic males with relatively low (A) and high (B) site-specific BV/TV throughout the hand. Note the similar distributions of relatively high BV/TV values at the dorsal aspect of the lunate, capitate head, palmar metacarpophalangeal joint, and dorsal interphalangeal joint.

1794 Figure 1.

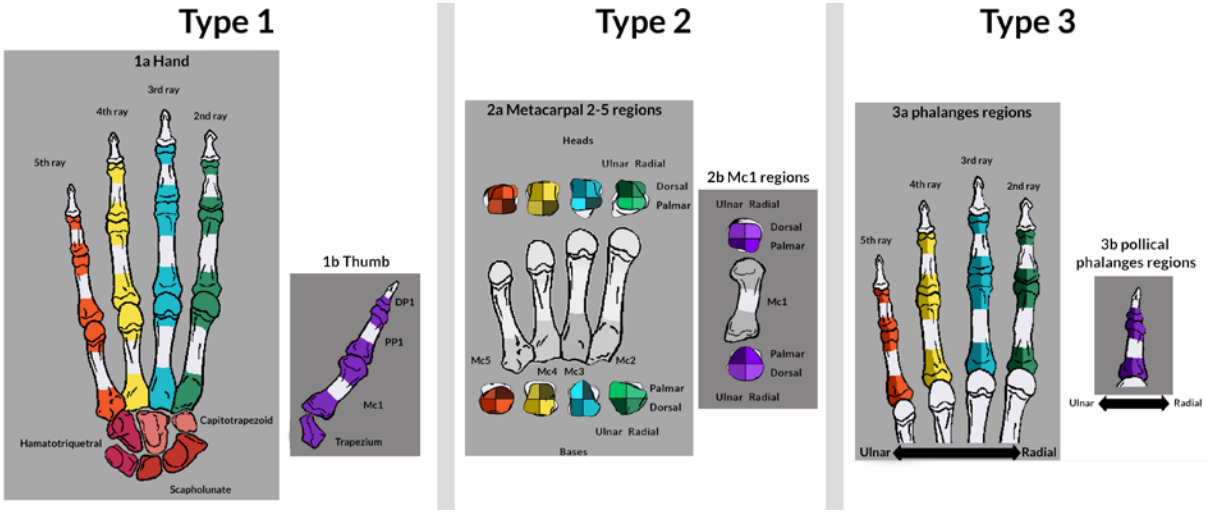

1795

1796

1797 Figure 2.

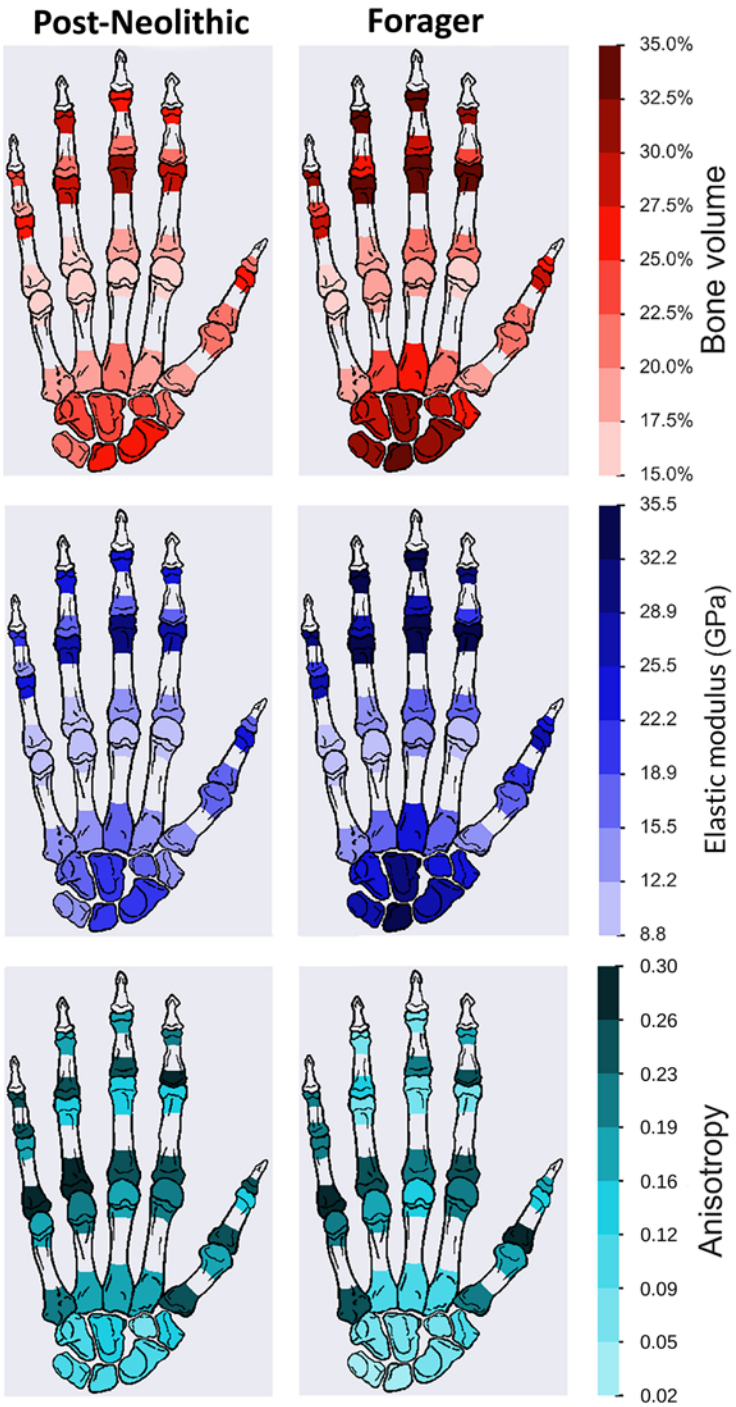

1798

1799

1800 Figure 3.

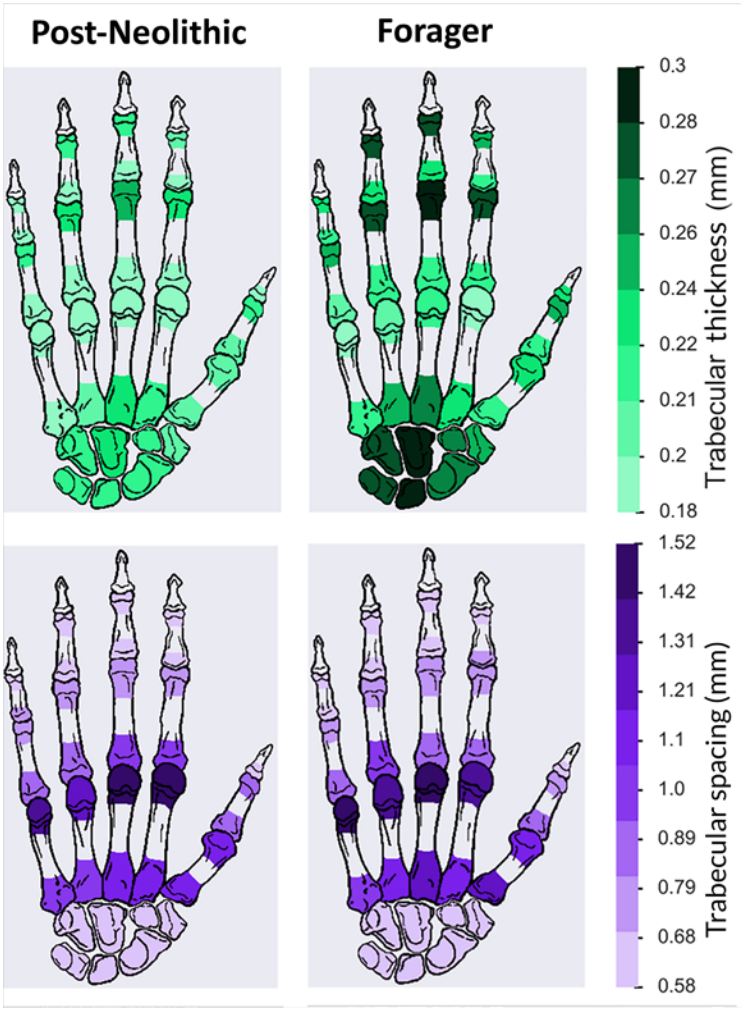

1801

1802

1803 Figure 4.

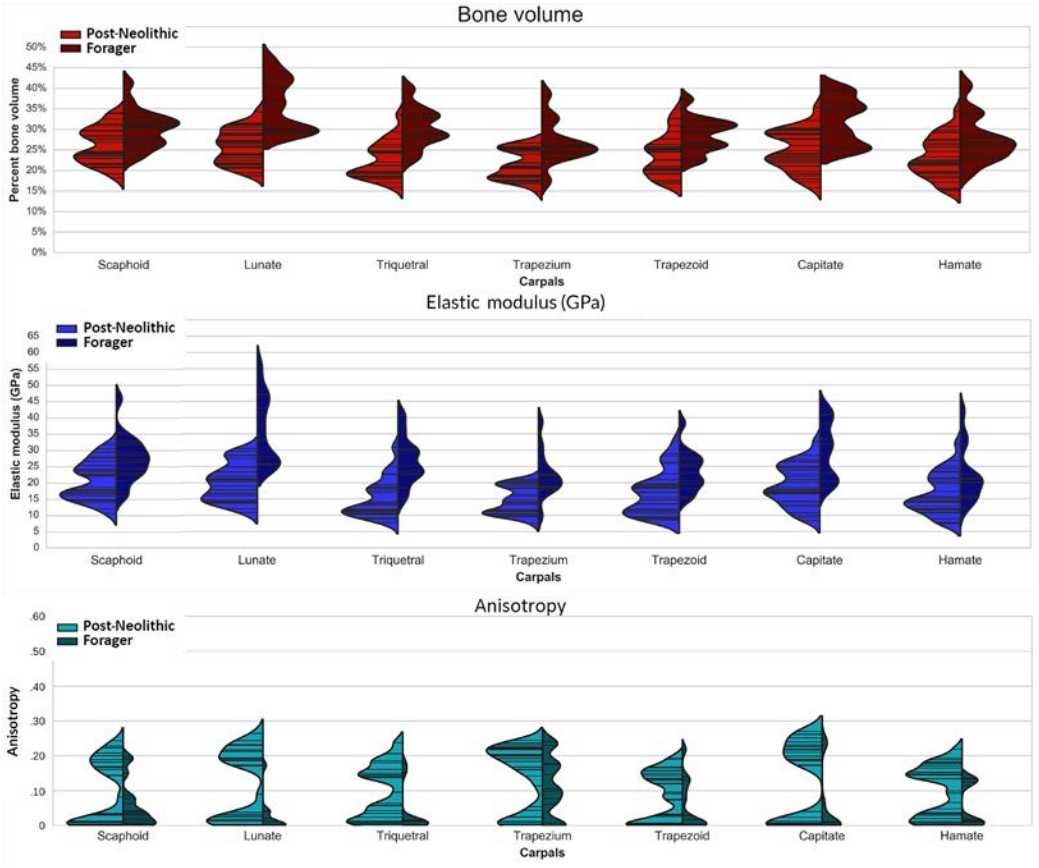

1804

1805

1806 Figure 5.

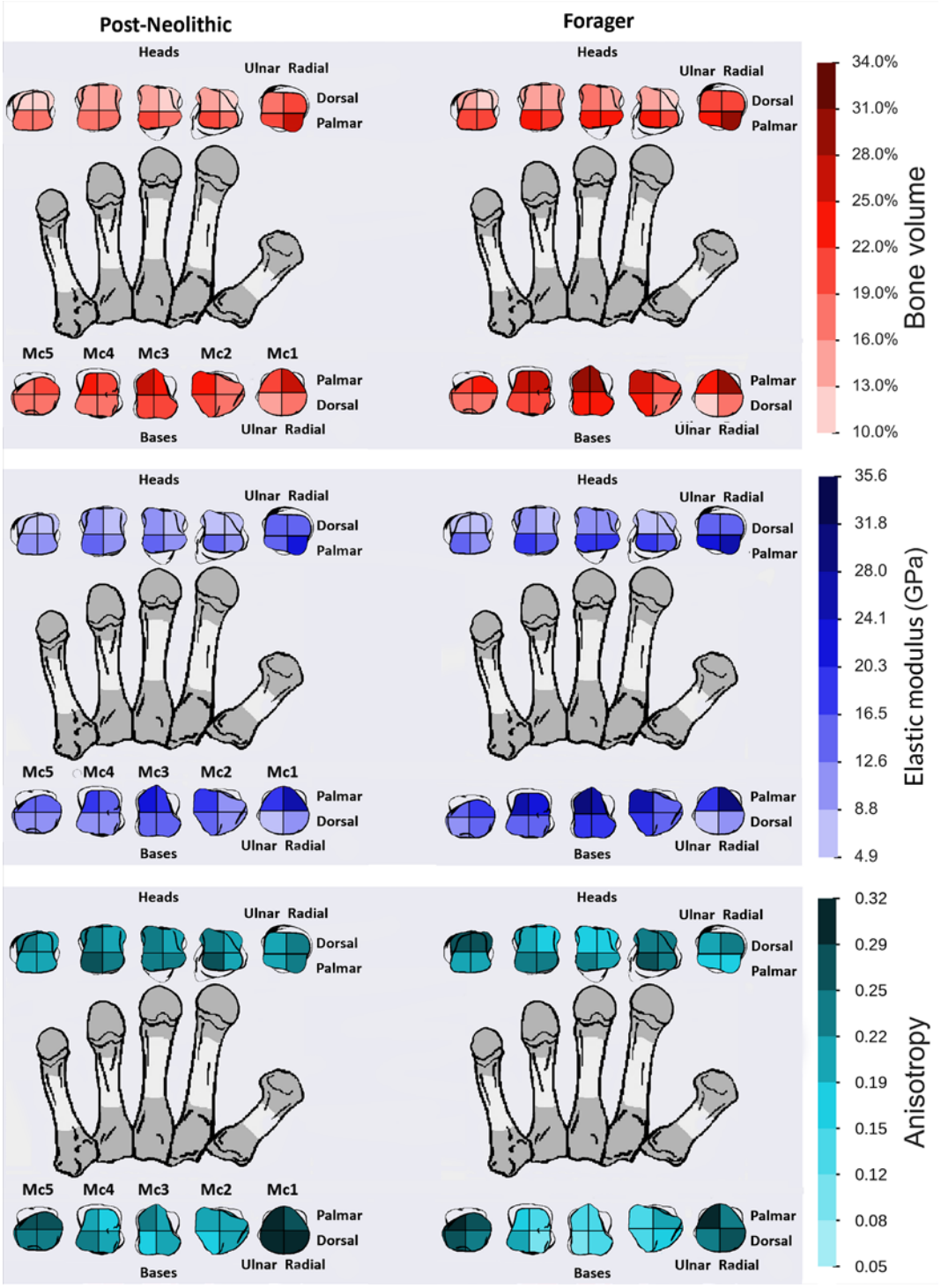

1807

1808

1809 Figure 6.

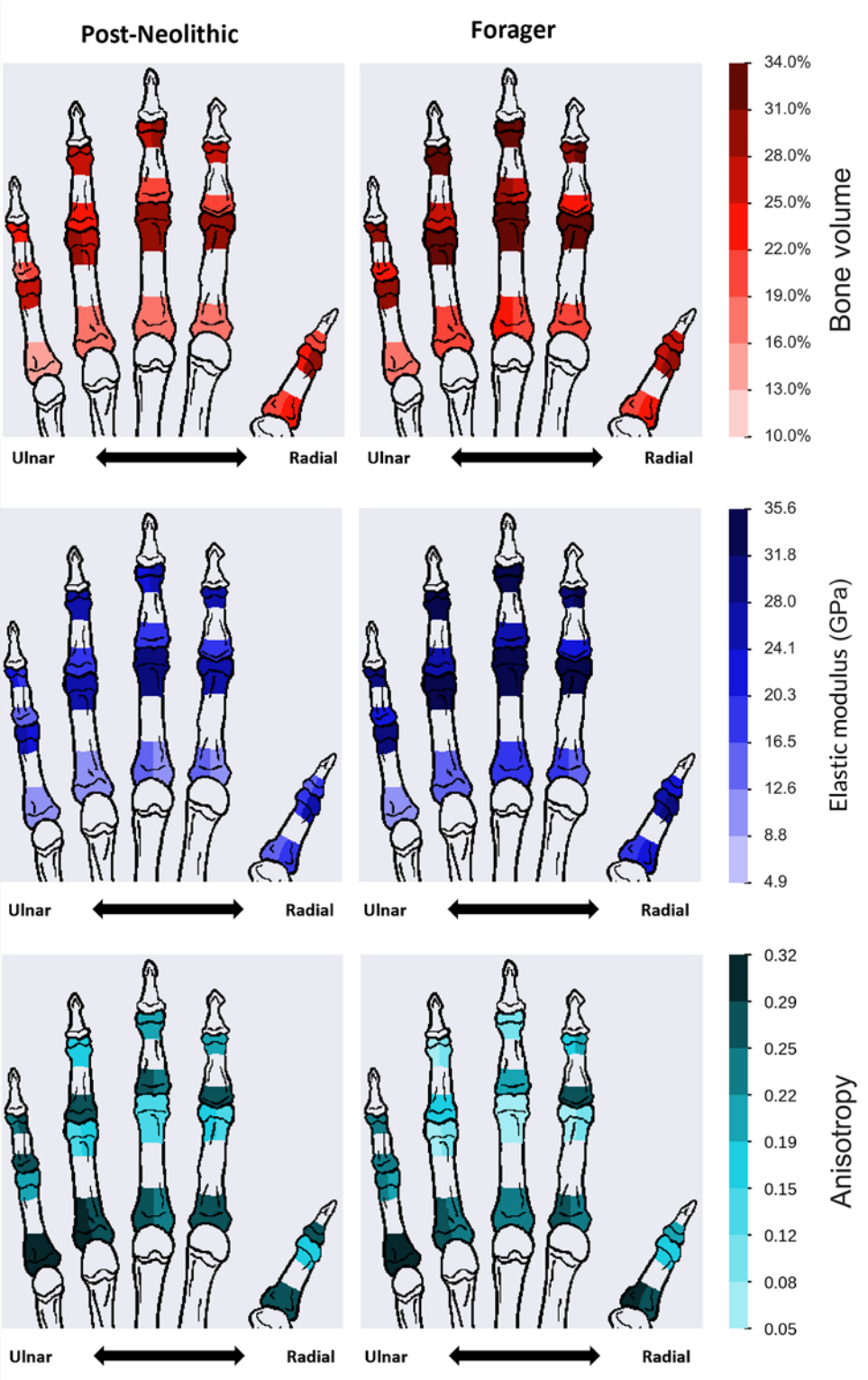

1810

1811

1812 Figure 7.

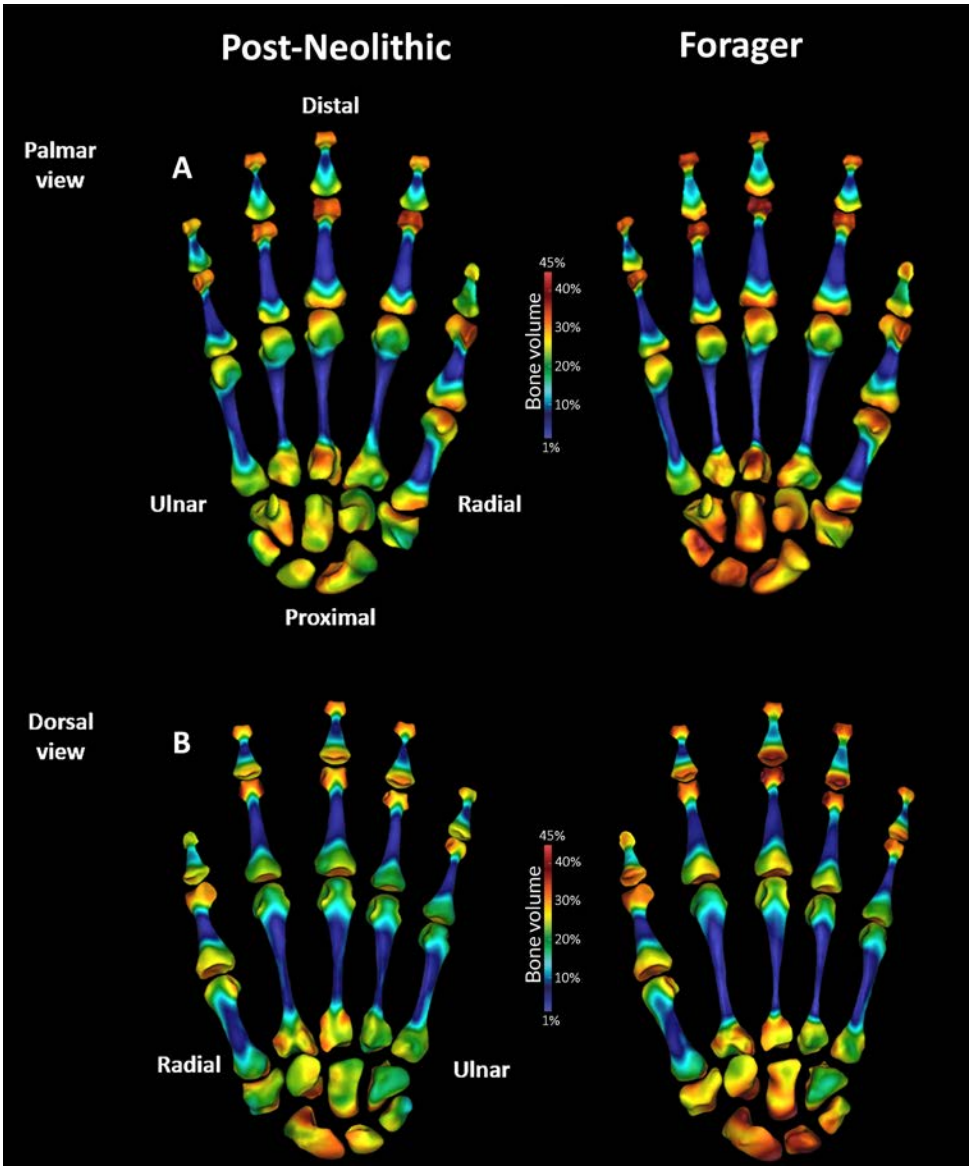

1813

1814

Figure 8.

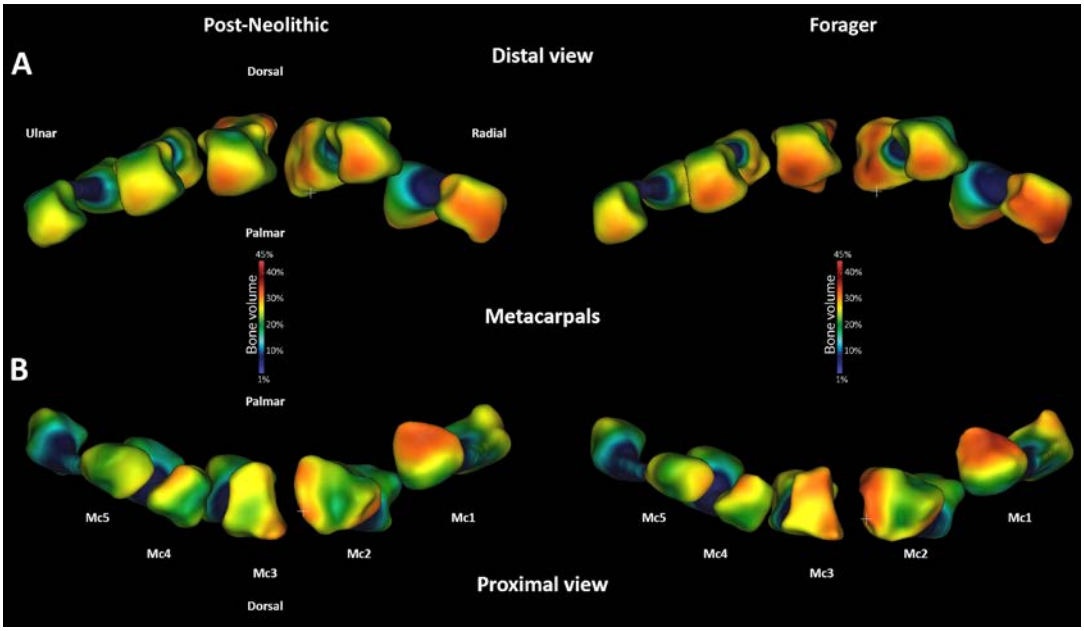
Post-Neolithic
Forager
A
Distal view
Dorsal
Ulnar
Radial
Palmar
45%
40%
30%
20%
10%
1%
Bone volume
Metacarpals
B
Palmar
Mc5
Mc4
Mc3
Mc2
Mc1
Proximal view
Dorsal

1818 Figure 9.

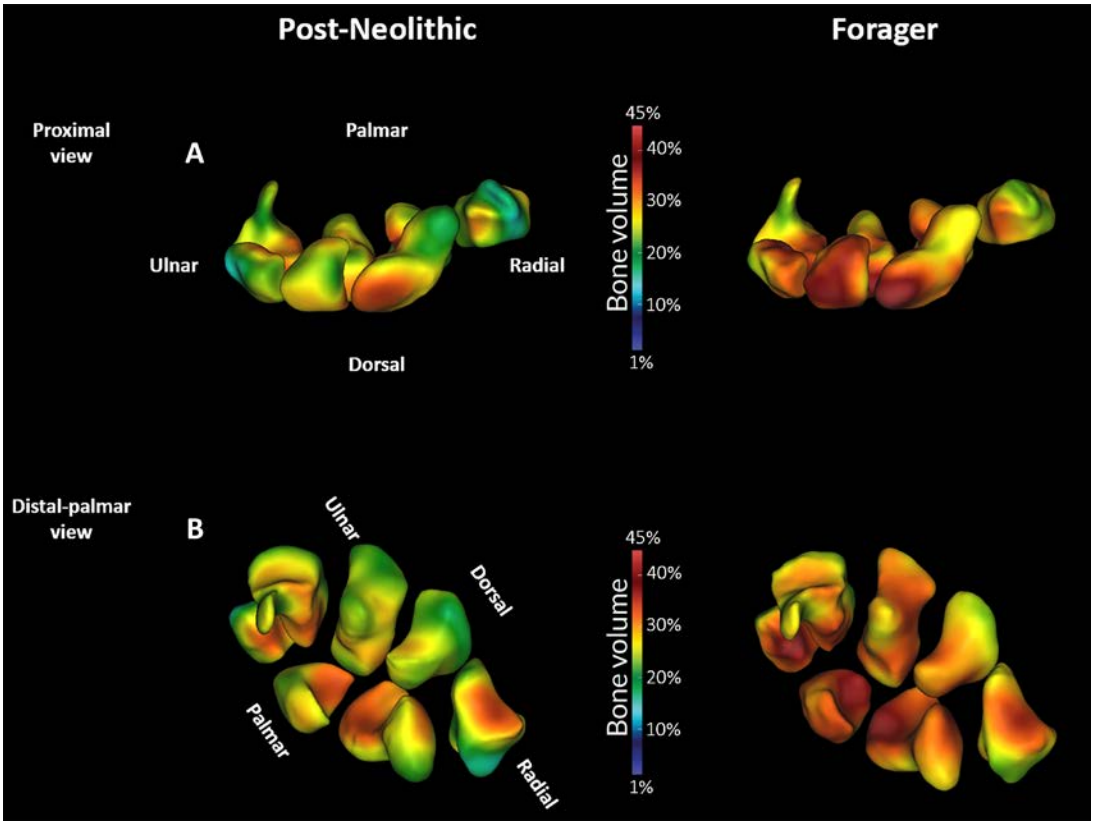

1819

1820

1821 Figure 10.

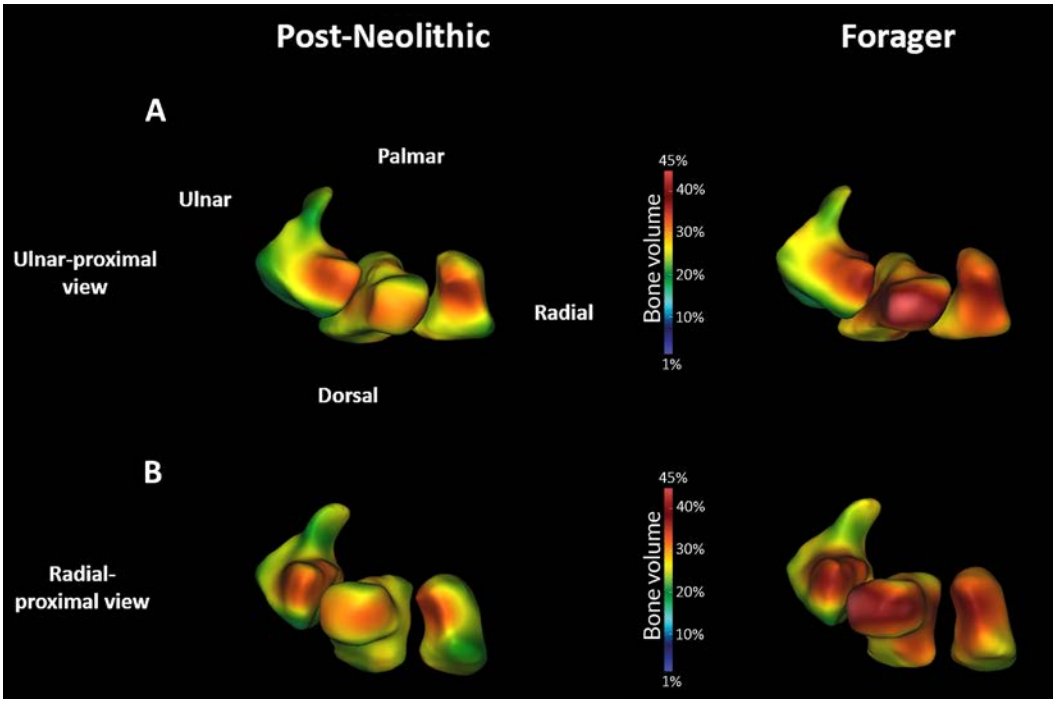

1822

1823

1824 Figure 11.

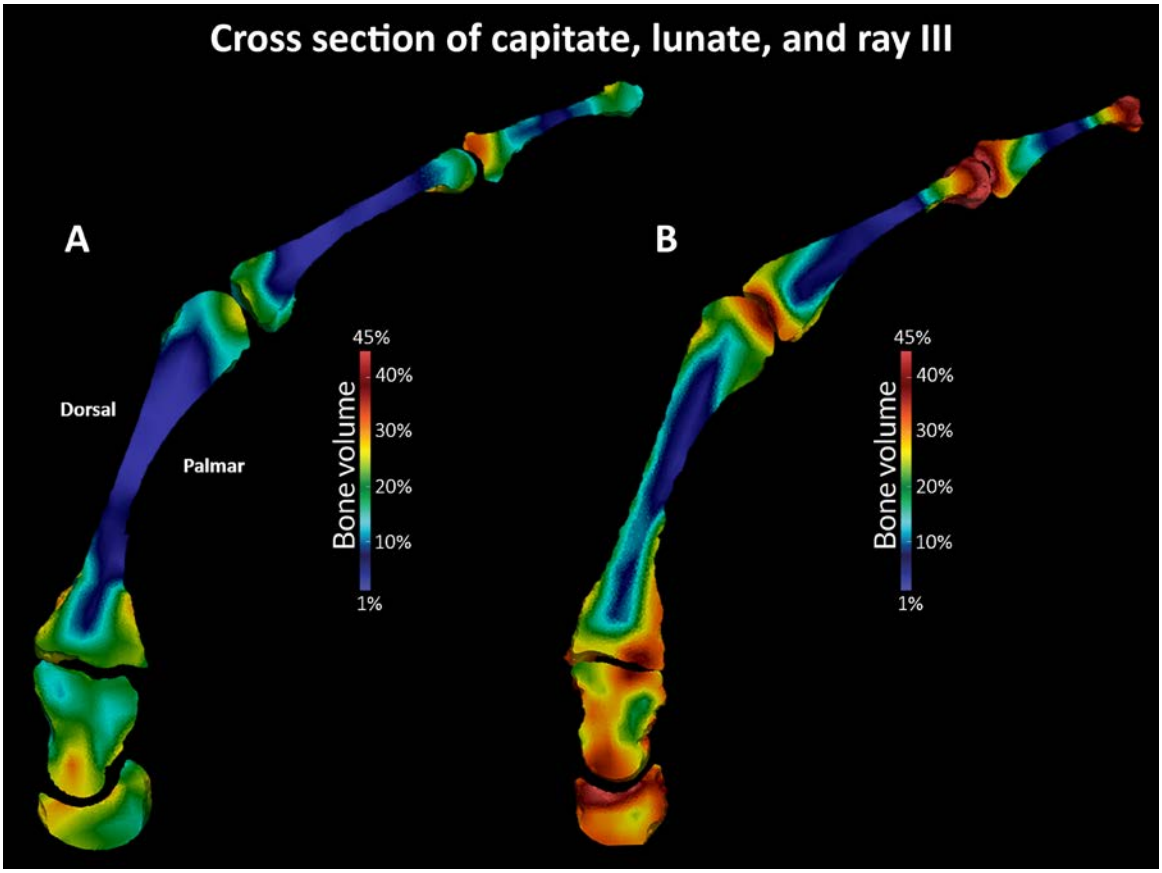

1825

1826

Table 1

Summary of manual elements per group.

Carpal	Total	PN	For.	Mc	Total	PN	For.	PP	Total	PN	For.	IP and DP	Total	PN	For.
Capitate	40	30	10	First	51	32	19	First	38	25	13	Distal first	39	27	12
Hamate	42	30	12	Second	55	32	23	Second	32	17	15	Second	37	24	13
Lunate	38	27	11	Third	55	33	22	Third	45	29	16	Third	44	31	13
Scaphoid	46	29	17	Fourth	47	33	14	Fourth	46	30	16	Fourth	37	24	13
Trapezium	41	29	12	Fifth	40	31	9	Fifth	42	29	13	Fifth	26	18	8
Trapezoid	43	30	13												
Triquetral	35	24	11												

Abbreviations: DP = distal phalanx; For. = number of bones in forager sample; IP = intermediate phalanx; Mc = metacarpal; PN = number of bones in post-Neolithic sample; PP = proximal phalanx; Total = combined number of bones within the sample.

Table 2

Summary of terms used within the linear mixed effect models and their predictions.[a]

Term	Definition
Sample	Post-Neolithic or forager
Skeletal element	The osteological designation of each bone (i.e., capitate, first metacarpal, etc.)
Segment	Unit of skeletal element analyzed. Specifically, whole carpal or subdivided region of a metacarpal/phalanx (i.e., carpal, base, or head)
Region	Subdivided metacarpal/phalangeal head or base segment:
	Metacarpal: dorsoradial, dorsoulnar, palmoradial, palmoulnar
	Phalanx: radial and ulnar
Region group	Used to group together the region measurements belonging to the same head or base: specimen + side + skeletal element + segment
Side	Side of the body a bone is from (i.e., right or left)
Specimen	Accession or individual identification (e.g., Qafzeh 8)
Hand ID	Identifier to distinguish the right and left hands of the same individual: side + specimen
Specific ID	Unique identifier used to prevent repeated analysis of a bone (pseudoreplication): Defined as skeletal element + specimen + side
Functional group	A grouping of functionally related skeletal elements and their respective segments/regions:
	Scapholunate: Scaphoid and lunate
	Capitotrapezoid: Trapezoid and capitate

	Hamatotrqiuetral:	Hamate and triquetral
	Thumb:	Trapezium, Mc1, first intermediate phalanx and the distal phalanx
	Ray II:	Mc2, and the second proximal and intermediate phalanx
	Ray III:	Mc3, and the third proximal and intermediate phalanx
	Ray IV:	Mc4, and the fourth proximal and intermediate phalanx
	Ray V:	Mc5, and the fifth proximal and intermediate phalanx
Model type 1	Contains data from carpals, thumb, and rays II-V head/base segments:	
Prediction	Similar distribution patterns for both samples, but the forager values will be significantly higher for BV/TV, E, and lower for DA.	
Model type 2	Contains data from Mc1-Mc5 head/base regions:	
Prediction	BV/TV and E distribution will reflect flexion and adduction/abduction, but the foragers' values will be significantly higher.	
Model type 3	Contains data from PP1-PP5 head/base, IP2-IP5 head/base, and DP1 base regions:	
Prediction	BV/TV and E distribution will reflect flexion at the interphalangeal joints, but the foragers' values will be significantly higher.	

Abbreviations: DP = distal phalanx; IP = intermediate phalanx; Mc = metacarpal; PP = proximal phalanx.

[a] Note that the functional groups for each model contain only the relevant segments and or regions (e.g., metacarpal regions are excluded from models testing only the differences between phalanges). See SOM S2 for a detailed description of each functional group. Note that the predictions for DA are not included because the models were rejected (see SOM S3 for details).

1832

1833